Article:
Paraskevopoulou, C orcid.org/0000-0002-7063-5592, Perras, M, Diederichs, M et al. (4 more authors) (2017) The three stages of stress relaxation - Observations for the time-dependent behaviour of brittle rocks based on laboratory testing. Engineering Geology, 216. C. pp. 56-75. ISSN 0013-7952

https://doi.org/10.1016/j.enggeo.2016.11.010

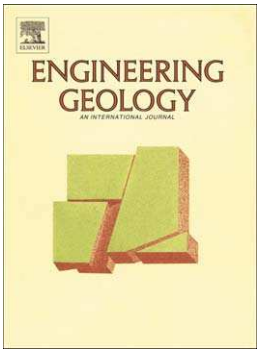

The three stages of stress relaxation - Observations for the time-dependent behaviour of brittle rocks based on laboratory testing

Chrysothemis Paraskevopoulou, Matthew Perras, Mark Diederichs, Florian Amann, Simon Löw, Tom Lam, Mark Jensen

PII: S0013-7952(16)30657-3
DOI: doi: 10.1016/j.enggeo.2016.11.010
Reference: ENGEO 4415

To appear in: *Engineering Geology*

Received date: 23 April 2016
Revised date: 16 September 2016
Accepted date: 16 November 2016

Please cite this article as: Paraskevopoulou, Chrysothemis, Perras, Matthew, Diederichs, Mark, Amann, Florian, Löw, Simon, Lam, Tom, Jensen, Mark, The three stages of stress relaxation - Observations for the time-dependent behaviour of brittle rocks based on laboratory testing, *Engineering Geology* (2016), doi: 10.1016/j.enggeo.2016.11.010

Title: The three stages of stress relaxation - Observations for the time-dependent behaviour of brittle rocks based on laboratory testing

Authors:
Chrysothemis Paraskevopoulou[1], Matthew Perras[2], Mark Diederichs[1], Florian Amann[2], Simon Löw[2], Tom Lam[3], Mark Jensen[3]

Corresponding Author:
Chrysothemis Paraskevopoulou
PhD Candidate
Department of Geological Sciences and Geological Engineering, Queen's University, Kingston, ON, Canada
email: chrys.parask@gmail.com, chrys.parask@queensu.ca, cparaske@ethz.c
telephone: +1 343 333 9241
address : 36 Union St., Miller Hall, Queen's University, Kingston, ON, Canada K7L3N6

Authors:
Matthew A. Perras
Research Associate and Lecturer in Engineering Geology
Institute of Geology, Swiss Federal Institute of Technology, Zurich, Switzerland
email: matthew.perras@erdw.ethz.ch

Mark S. Diederichs
Professor
Department of Geological Sciences and Geological Engineering, Queen's University, Kingston, ON, Canada
email: diederim@queensu.ca

Florian Amann
Senior Scientist
Institute of Geology, Swiss Federal Institute of Technology, Zurich, Switzerland
email: florian.amann@erdw.ethz.ch

Simon Löw
Professor
Institute of Geology, Swiss Federal Institute of Technology, Zurich, Switzerland
email: simon.loew@erdw.eth.ch

Tom Lam
Nuclear Waste Management Organization, Toronto, Ontario, Canada
email: tlam@nwmo.ca

Mark Jensen
Nuclear Waste Management Organization, Toronto, Ontario, Canada
email: tlam@nwmo.ca

Affiliations:
[1] *Department of Geological Sciences and Geological Engineering, Queen's University, Kingston, ON, Canada*
[2] *Institute of Geology, Swiss Federal Institute of Technology, Zurich, Switzerland*
[3] *Nuclear Waste Management Organization, Toronto, ON, Canada*

Key words:
time-dependent behaviour, time-dependency, stress relaxation testing, laboratory testing, stages of stress relaxation, brittle rocks,

1 INTRODUCTION (WAS SIMPLIFIED SOME PARTS WERE REMOVED, ACCORDING TO REVIEWER #1)

Time-dependent behaviour of rock and time-dependent testing methods have been well studied by many authors at both the laboratory and the tunnel scale (e.g. Wawersik, 1972; Rutter et al. 1978; Chen and Chugh, 1996; Boukharov et al. 1995; Brantut et al. 2013; Ghaboussi and Gioda 1977; Malan, 2002; Schubert et al. 2003; Barla et al. 2010). Time-dependent behaviour of rock masses have also been studied for landslides (Bizjak and Zupanic, 2007) and forms an important aspect of the predicted and observed movement of many landslides (Groneng et al. 2010). In a tunnelling environment, long-term time-dependent behaviour can lead to severe deformation at significant distances behind the face, impacting ground support performance, tunnelling logistics, and under-estimated preliminary and design stage project costs (Paraskevopoulou and Benardos, 2013). Time-dependent deformation and behaviour is also important in the shorter-term, in terms of delayed strain evolution and stress migration within the near-face region of the tunnel, affecting the optimal timing of support installation and interpretation of monitoring data. However, in practice most site characterization and laboratory testing focuses on material properties including strength and deformability within the short (practically instantaneous) time constraints of standardized testing (ISRM, 1979). The stability and safety of underground excavations requires such experimental data for numerical prediction of rock behaviour. Challenges may arise when dealing with in situ stress conditions where time-dependency issues, such as consolidation, swelling, squeezing, creep or stress relaxation, take place or when multiple mechanisms occur simultaneously. Goodman (1980) highlighted the importance of including time as a parameter of rock behaviour analysis.

The purpose of this paper is to give insight into the time-dependent behaviour of brittle rock materials and the importance of performing laboratory testing, such as stress relaxation tests, which can be used to determine parameters for input into numerical simulations. This study focuses on two different types of limestone; the Jurassic limestone from Switzerland, and the Cobourg limestone from Canada. In the first phase of testing, the Jurassic limestone was used to examine the testing procedure and the key parameters to be monitored during testing. In a second phase of testing the time-dependent behaviour of the Cobourg limestone, which is the potential host rock for a proposed Low and Intermediate Nuclear Waste Repository in Canada, was examined. According to Damjanac and Fairhurst (2010), a better understanding of the long-term rock deformability in the design and construction of nuclear waste repositories is a key behavioural aspect for predicting the ability of the rock to isolate the waste from the biosphere.

2 BACKGROUND (SIMPLIFIED, PARAGRAPHS WERE REMOVED, ACCORDING TO REVIEWER #1)

2.1 Definitions

Time-dependent phenomena can be defined as mechanisms resulting in deforming or weakening the rock mass over time. In the literature (Barla, 1995; Aydan et al. 1993; Einstein, 1996; Singh 1975) the most widely discussed time-dependent phenomena associated with tunnelling are creep, consolidation, dilation and swelling. Creep involves time-dependent distortion (shear strain) without volume change and can result from many complex mechanisms at the atomic or grain scale. Consolidation is a volume decrease involving the redistribution of pore fluids or the collapse of pores and open defects. Dilation is the opening of fractures, pores and defects due to numerous mechanisms including crack damage and dilational shear (with or without fluid migration). Swelling is a volume change that occurs due to physio-chemical changes within the rock leading to expansion. These mechanisms can manifest themselves as apparent visco-elastic (recoverable, time-dependent) behaviour or visco-plastic (non-recoverable, time-dependent) behaviour. For simplified loading paths, visco-elastic models can be combined and configured (eg. Lo and Yuen, 1981) in order to phenomenologically simulate actual deformation that mechanistically may not be purely elastic. Conversely, mechanistic visco-plastic models can be employed with associated increase in parametric complexity (eg. Barla et al. 2010).

Tunnel squeezing (Barla, 1995) is an observable result of one or more of the mechanisms above and is the inelastic closure of the tunnel profile with or without tunnel advance. Some component of total squeezing can be instantaneous (in practical terms) as a result of short-term inelastic response to stress change (shearing, dilation), observable after each increment of tunnel advance. Components of the total deformation may also be delayed due the time-dependent phenomenon discussed above.

If the support installation is delayed, the rock mass moves into the tunnel and stress redistribution takes place around it. In contrast, if deformation is restrained through support installed close to the face, squeezing will lead to delayed load build-up acting on the rock support system. This build-up will occur regardless of when the support is installed, however, the magnitude depends on the timing of the support installation (Hoek et al. 2008; Hoek and Guevara, 2009). Time-dependency can affect the tunnel and support system within the time-frame of the excavation cycle or it can be observed to continue long after support completion and tunnel advance.

Moreover, during the life span of an underground project, other mechanisms of time-related effects may take place and influence or change the properties of the excavation damage zone. This is particularly important in cases where flow through the damage zone is to be minimized, such as for the case of a nuclear waste repository (Backblom and Conrox, 2008).

2.2 Time-Dependent Models

Researchers generally examine the above mechanisms and responses through laboratory testing, analytical methods utilizing rheological models comprised of mechanical analogues and/or empirical models based on curve fitting of experimental data, (Goodman, 1980). The idealized creep behaviour is often represented mathematically by the Burger's model, which is in fact the combination of the Kelvin (delayed manifestation of a constant static response to altered boundary conditions) and Maxwell (continued strain rate or relaxation over time under static boundary conditions) models in series (as illustrated in Fig. 1). Deformation that occurs at constant loading condition through time can be expressed using Eq. 1 (Goodman, 1980), where: ε_1 is the axial strain, σ_1 is the constant axial stress, K is the bulk modulus, η_K is Kelvin's model viscosity, η_M is Maxwell's model viscosity, G_K is Kelvin's shear modulus, G_M is Maxwell's shear modulus. η_K, η_M, G_K, G_M are the visco-elastic parameters and are considered properties of the rock.

$$\varepsilon_1(t) = \frac{2\sigma_1}{9K} + \frac{\sigma_1}{3G_M} + \frac{\sigma_1}{3G_K} - \frac{\sigma_1}{3G_K} e^{-(\frac{G_K}{\eta_K}t)} \quad \text{(Eq. 1)}$$

During stress relaxation the strain-state is controlled and remains constant, thus rearranging Eq. 1 for a constant strain component, the material's stress state is changing according to Eq. 2.

$$\sigma_1(t) = \varepsilon_1[G_M e^{-\left(\frac{G_M}{\eta_M}t\right)} + G_K e^{-\left(\frac{G_K}{\eta_K}t\right)}] \quad \text{(Eq. 2)}$$

Maxwell and Kelvin models are also mechanical analogues of linear visco-elastic bodies simulating different material behaviour; when in series however, they comprise the Burger's model that is commonly used to simulate creep behaviour.

The Burgers model parameters can be derived from creep test results by fitting the components to the laboratory data following Goodman's (1980) approach, for example. According to Goodman, the visco-elastic parameters (η_K, η_M, G_K, G_M) can be estimated by fitting the experimental results of static load (creep) tests to the mathematical curve of the strain response of the Burgers model at different time increments and the corresponding strain intercepts.

In reality and embedded in this mathematical concept are the three stages of creep (summarized by Goodman 1980) that follow the instantaneous response (0^{th} stage) to changed

boundary conditions resulting to a constant stress-state. These stages can be interpreted and simulated as follows:

- 1st stage or primary or transient creep where the delayed adjustment to a new equilibrium state takes place through visco-elastic (reversible) deformation, and may be accompanied by some irreversible behaviour, resulting in strain accumulation with decreasing rate over time. This stage is commonly simulated with the Kelvin model analogue.
- 2nd stage or secondary creep where the material exhibits a consistent strain accumulation rate over time accompanied by inelastic distortion. The duration or even existence of this stage can vary depending on the ability of the rock type to transition from ductile to more brittle materials. The Maxwell visco-elastic model is commonly used to phenomenologically represent this stage.
- 3rd stage or tertiary creep where strong non-linear or accelerating strains occur (typically driving the material to rupture) due to strain-driven weakening, chemically related strength degradation and/or interaction of growing cracks. Visco-plastic models (Barla et al. 2010) and/or so-called stress corrosion models (Damjanac and Fairhust, 2010) are used to simulate tertiary creep.

A combination of Kelvin and Maxwell model components is referred to as the Burgers model which can be used to simulate stages 1 and 2 in combination.

The three stages of creep have been well studied and occur for many materials and rock types (Scholz, 1968; Borchert et al. 1984; Goodman, 1980; Ottosen, 1986; Zheng and Weng, 2002). This conceptual model applies also to relaxation testing data. Therefore, by changing the boundary conditions of a creep test to a constant strain boundary, conceptually there should also be three stages of stress relaxation. Adopting the approach described by Goodman (1980), of determining parameters from static load (creep) tests, the same parameters (i.e. viscosities and shear moduli) should be derivable from stress relaxation tests, assuming that the rock material is behaving as a linear visco-elastic Burger's body in unconfined compression (illustrated in Fig. 1).

The testing and analysis presented herein focus on stress relaxation testing, i.e., the time-dependent response of rock under constant (controlled) strain, to understand the behaviour at the laboratory scale and to verify the hypothesis of three stages of stress relaxation.

2.3 Damage Evolution and Failure of Brittle Rocks

The stress relaxation tests were conducted at different axial strain levels which were representative of driving stress to strength ratios that were determined from baseline Unconfined Compressive Strength (UCS) testing. UCS testing is governed by the suggested method from the ISRM (1979) guidelines. Initial analysis was conducted using an average UCS value from the baseline data and more detailed analysis was conducted using the damage thresholds, described below, from each individual stress relaxation test.

Ductile deformation processes, including those conventionally associated with creep in geological materials, involve continuum processes such as dislocation slip or migration of interstitial atoms and atomic vacancies within crystals, or weak bond migration in clay minerals (Davis et al. 2012). Such deformation results in distortion (pure or simple shear strain) over time.

In brittle rocks, however, it is generally accepted that a progressive damage process governs the failure, which is initially dominated by the initiation and propagation of microcracks in the direction of the maximum load (Fairhurst and Cook, 1966). In this sense, the primary manifestation of the initial progressive damage process is non-linear radial extension associated with comparatively negligible inelastic strain response in the axial loading direction (Bieniawski, 1967).

The stages of the brittle failure process include at least four distinct stages that can be identified if the stress-strain response is monitored during loading, as shown in Fig. 2. The stages are: i.) closure of pre-existing cracks; ii) linear elastic behaviour; iii) stable crack growth; and iv) unstable crack growth, which leads to failure and the peak strength (the point of maximum stress). Stable crack growth involving cracks aligned parallel to the primary loading direction initiates at a stress-level that can be defined by analysis of radial strain or acoustic emissions (Brace et al. 1966; Lajtai, 1998; Eberhardt, 1998; Diederichs et al. 2004). Unstable crack growth in a UCS sample begins when isolated microcracks interact at a critical crack density (or critical radial strain) or when conditions exist for propagation of individual cracks significantly beyond the grain dimension (Martin, 1993; Diederichs, 2003) and ultimately leads to failure. These damage or crack growth thresholds have been defined by the International Rock Mechanics Committee on Spall Prediction as CI and CD respectively (Diederichs and Martin, 2010).

Stress-strain curves for brittle rocks can be used to determine the: i) crack initiation stress (CI); ii) critical damage stress or axial yield stress (CD); and, iii) uniaxial compressive strength (UCS).

Many researchers (Bieniawski, 1967; Martin and Chandler, 1994; Martin, 1993; Lajtai, 1998; Eberhardt, 1998, Diederichs, 1999 and 2003; Diederichs et al. 2004; Diederichs and Martin, 2010, Nicksiar and Martin, 2012; Ghazvinian, 2015) investigated the identification of the thresholds using various methods (i.e. strain-based or acoustic emission). For instance, the Crack Initiation (CI) threshold can be determined as the axial stress at reversal point of the calculated crack volumetric strain according to Diederichs and Martin's (2010) approach. The deviation from linearity of the radial strain is another approach used to determine CI (Bieniawski, 1967; Lajtai, 1974; Diederichs et al. 2004), which is free from errors introduced by involving calculated parameters in the estimation. Critical Damage (CD), the crack coalescence and interaction threshold (Lockner et al. 1992), is determined as the axial stress at the measured volumetric strain reversal point (Bieniawski, 1967; Lajtai, 1974; Martin, 1997).

Crack initiation (CI) in a compressive test marks the beginning of the stress-induced damage process in low porosity brittle rocks. Beyond this point, the cracks initiate in an isolated fashion at locations where local imperfections lead to internal tensile stress concentrations (Griffith, 1924; Brace et al. 1966; Fonseka et al. 1985). These cracks extend for a limited distance in the load parallel direction (releasing acoustic emissions and contributing to a non-linear increase in radial strain as load is increased. At increasing stress levels between CI and CD the cracks accumulate and grow in a stable manner, with the process arrested in the short-term by a halt in the load increase. If the load or axial stress is held constant between these thresholds, however, time-dependent crack growth occurs leading to time-dependent deformation, as illustrated in Fig. 2. Loading above the critical damage threshold (CD) marks the growth of cracks in an unstable manner during unconfined compressive testing. If the axial stress is maintained at a stress level in excess of CD, accelerated creep rates may occur that can lead to a sudden failure of the specimen (Schmidtke and Lajtai, 1985).

Many researchers (Brace et al. 1966; Podnieks et al. 1968; Beniawski, 1967; Martin, 1997; Diederichs, 2003, etc.) investigating the inelastic behaviour of rocks indicated that crack initiation and propagation plays a dominant role in understanding processes related to time-dependent behaviour. Stress relaxation is one of the phenomena associated with the inelastic behaviour of rocks, for which the role in rock mechanics has so far only been studied by a few authors (Peng, 1973; Rutter et al. 1978; Engelder, 1984; Lodus, 1986). This testing method should also be influenced by crack initiation and propagation processes.

2.4 Stress Relaxation of Rocks – Previous Work

According to Hudson and Harrison (1997) creep is defined as increasing strain while the stress is held constant whereas stress relaxation is defined as decreasing stress while the strain is held constant. In practice, and especially for the rock near an underground excavation, a rock element will undergo stress and strain changes during construction and the strain is largely controlled by the stiffness of the adjacent rock. Time-dependent behaviour will initiate immediately after excavation and the boundary conditions of rock elements near the excavation will be somewhere between the ideal conditions (i.e. constant stress or constant strain) leading to creep and stress relaxation, depending on the location around excavation (Hudson and Harrison, 1997).

The rock around an underground opening redistributes from a primary stress-state to a secondary stress-state. As the stress concentration increases during excavation, failure of the rock may occur and an excavation damage zone develops. After excavation, the rock is then subjected to this secondary stress-state for a long period of time where time-dependent processes may take place, influencing the long-term behaviour of the rock and the properties of the damage zone.

According to Peng and Podnieks (1972) relaxation is the time-dependent behaviour of stress within a stressed elastic body. It can be demonstrated by holding the deformation constant in the conventional compressive strength test. To examine the phenomenon of relaxation Peng and Podnieks (1972) performed relaxation tests on tuff specimens. The testing procedure involved holding the specimen at constant deformation at points along the stress-strain curve. The testing results showed that no load drop was observed for samples loaded below stress levels where the stress-strain curve deviates from linearity (i.e. below the Crack Damage threshold). However, for points above CD a small load drop was observed and the magnitude of the load drop increased as the applied load increased. They concluded that the stress relaxation seems to be closely related to the formation and propagation of cracks.

Peng and Podnieks (1972) also noted that below CD no stress relaxation was observed due to the fact that the surfaces of the pre-existing microcracks in that region were too small to cause any appreciable load drop. In addition, Peng (1973) suggested that load relaxation tends to stabilize the fracture growth within the specimen. More specifically, as the axial deformation is held constant no external energy is imposed on the specimen, consequently when cracks start to initiate the load bearing capacity drops and the load must be reduced to prevent any axial displacement from taking place.

Peng (1973) also examined the relaxation behaviour on three rock formations: Arkose sandstone, Tennessee marble and Berea sandstone. The load was increased until a macro-crack initiated in the post-failure region. The strain was then held constant and the stress drop was monitored. When the stress relaxation attains an asymptotic level as shown in Fig. 3 then, as Peng (1973) stated, the stabilization of crack propagation is achieved. In addition, the relaxation behaviour of rock indicates that the fractured rock will attain new equilibrium if sufficient time is given for load relaxation to occur.

Lodus (1986) examined how the rate of drill-ability during excavation correlates with the stress relaxation pattern within the rock mass by conducting relaxation tests on potassium salt and marble under uniaxial compressive loading conditions. The results showed that the materials exhibited more relaxation when subjected to higher stress levels, as shown in Fig. 3. Lodus (1986) concluded that the energy release due to stress relaxation in an underground opening could be controlled by reducing the speed of the mechanical tool into the working face and could be directly evaluated from data acquired from relaxation testing.

Li and Xia (2000) performed a series of relaxation tests in uniaxial compression on a red sandstone, from the Emei Mountain area in the Sichuan province of China, and claystone, from the Shenbei coal field in the Liaoning province of China, which are shown in Figure 5-3. It was observed from their study that both rock types when subjected to stress levels above 75% of their uniaxial compressive strength failed under constant strain conditions but still exhibited residual resistance. Li and Xia (2000) suggested that this observation could be used to interpret the behaviour and assess the load bearing capacity of the pillars in mine sites.

3 LABORATORY TESTING PROGRAM AND METHODS

3.1 Sample Descriptions

The selected Jurassic limestone comes from a quarry north of Zurich, Switzerland, in the tabular Jura (Fig. 4.a). The samples are a fossile rich packstone, following the classification system of Dunham (1962), with variable sized vugs ranging from 0.1 – 3 mm and pyrite rich crystal patches. There are also lime-mudstone blebs ranging from 5 – 30 mm in diameter, mixed within the packstone framework. 55.6 mm diameter samples were cored from a block measuring 500 x 500 x 150 mm, such that the core long axes (before end face grinding) were 150 mm long. All the samples were prepared according to the ISRM (1979) requirements.

The Cobourg limestone (Fig. 4.b) comes from the Bowmanville quarry, near Bowmanville, Ontario, Canada. It is Middle to upper Ordovician in age and also known as the Lindsay

Formation in south-central and eastern Ontario. It is of very low porosity, typically < 2% total porosity (Sterling et al. 2011). The limestone has a characteristic mottled texture, with the light gray areas being a fossil rich lime-packstone and the dark gray being argillaceous lime-mudstone. A block measuring 400 x 400 x 700 mm was cored perpendicular to the irregular bedding marked by the argillaceous banding. Due to the limited volume of material for testing, not all samples were 150 mm long (before end face grinding), such that the height to diameter ratio ranges between 2.0 and 3.0. All other sample preparation procedures were conducted according to the ISRM (1979) requirement.

3.2 Baseline Testing

Baseline Unconfined Compressive Strength (UCS) tests were conducted on 10 cylindrical samples of Jurassic limestone and 9 cylindrical samples of Cobourg limestone. A modified 2000 kN Walter and Bai servo-controlled rock testing device was utilized. Load was applied in such a way as to maintain a constant radial displacement rate of 0.01 mm/min. Radial displacement was measured using single strain gauge that was attached to a chain wrapped around the mid height of the specimens and the axial strain was measured on the sample surface using two strain gauges at opposite sides of the specimen.

3.3 Determination of brittle stress thresholds

Baseline Unconfined Compressive Strength (UCS) testing was performed on both Jurassic limestone and Cobourg limestone to determine the damage thresholds, Crack Initiation (CI) and Critical Damage (CD), and the peak strength using strain based methods. Several methods were adopted to determine CI and CD values. More specifically, Lajtai's (1974) radial strain method and Diederichs and Martin (2010) crack volumetric strain approach were used to determine CI thresholds and Lajtai's (1974) axial strain method and Bieniawski's (1967) volumetric strain reversal method were used for CD respectively in UCS tests. The results were used to determine the load levels for the relaxation testing series.

From the relaxation testing the data collected during the initial loading were used to determine the Crack Damage thresholds and elastic properties where applicable (i.e. those loaded above CI). The damage thresholds identified in the relaxation tests, using Lajtai's (1974) methods, were closer to the baseline values estimated from UCS testing.

3.4 Defining strain thresholds

The driving stress-ratio has been defined as the axially applied stress level, at a particular stage in the test, normalized to the average UCS (so-called instantaneous response measured

according to ISRM, 1979 standards) and has been used by many other researchers (Schmidtke and Lajtai, 1985; Lajtai et al. 1991; Lau and Chandler, 2004; Potyondy, 2007; Damjanac and Fairhurst, 2010) to present long-term (time-dependent) testing results acquired from creep tests. In order to determine the desired (target) load stress for the start of the relaxation test, the results from the UCS testing (baseline samples) were used as a reference to find the equivalent axial displacement or radial displacement (to be used for machine control) in the relaxation tests. The actual stress level in the sample used for relaxation testing differed (due to material variability) from the target value by +/- 0.05 to 0.1 MPa, depending on the sample.

3.5 Relaxation Testing under Compression and Testing Procedure

The procedure of the relaxation testing performed and presented in this paper was adapted from the ASTM (2013) guidelines for structural elements to make it applicable to rock testing. There is not a suggested testing method for relaxation testing on rocks available from the ISRM. During the relaxation testing series the lab conditions were monitored and it should be noted that overall the temperature and humidity conditions were generally maintained within a range with an average total change of +/- 0.7 ^{o}C and 3.5%, respectively.

The first goal of the testing program was to examine the most appropriate method to conduct a relaxation test on a servo-controlled uniaxial testing machine (Walter and Bai - 2000kN). The stress relaxation behaviour was examined under both axial strain-controlled and radial strain-controlled conditions. In the former case, the axial strain was kept constant when the desired load was reached while in the latter case the radial strain was kept constant. Multi-step and single-step load tests were conducted. All tests have been performed at stress levels between CI (or close to CI) and CD. Table 1 summarizes the samples that were tested under the various conditions.

Two test series have been performed: in a first series Jurassic limestone was utilized to examine the applicability of various testing procedures (i.e. axial strain-controlled, radial strain-controlled, multi-step and single-step) for assessing the long-term relaxation behaviour. As a consequence of the analysis of the first test series, the second test series on Cobourg limestone was performed utilizing a single-step axial strain-controlled testing procedure.

3.5.1 Axial strain-controlled relaxation tests

3.5.1.1 Multi-step

Multi-step tests were first conducted on 2 Jurassic limestone samples to understand the behaviour without using many samples. Both consisted of 10 different load levels with the

second test load levels overlapping but becoming higher than the first test. The duration of each level varied from 6 hours to just over 24 hours. The hold time during each test depended on the sample's behaviour; and the test was terminated when the load had reached a constant value where no further load decay (relaxation) was observed.

3.5.1.2 Single-step

Single-step load tests at comparable driving stress ratios as the multi-step load levels were conducted on14 samples of Jurassic limestone and 16 samples of Cobourg were tested. It should be stated that the Jurassic samples needed less time to reach linearity in terms of stress relaxation than the Cobourg samples. As a general trend the Jurassic limestone relaxed within 6 to 24 hours and the Cobourg limestone needed at least 24 to 48 hours, depending on the stress level to which the sample was subjected.

3.5.2 Radial strain-controlled relaxation tests

3.5.2.1 Multi-step

Another aspect of the testing series presented herein was to examine the rock's relaxation response under radial strain-controlled conditions where the radial strain was kept constant and the axial stress and axial strain were monitored. This testing series included only 3 multi-step tests on Jurassic limestone samples. All of the samples were tested at different load levels, two samples were each tested under eight different load levels and one under two load levels. The hold time differed as the relaxation response of the material under constant radial strain varied more significantly than the axial, as discussed in the following sections.

4 LABORATORY RESULTS

4.1 Baseline testing and Damage thresholds

The stress-strain relationships of the 10 UCS tests on Jurassic and the 9 UCS tests on Cobourg limestone are shown in Fig. 5, top and bottom, respectively. The average values estimated for UCS, CD and CI were 103 MPa, 91 MPa, 39 MPa respectively for the Jurassic limestone and 125 MPa, 111 MPa and 50 MPa for the Cobourg limestone. The results are summarized in Table A.1 (see Appendices).

4.2 Relaxation Testing

Selective results are presented in this section serving as examples to describe the main influencing factors during the relaxation process of the two rock types. In these tests, a target

constant axial or radial strain is achieved and maintained by controlling the applied axial force (allowing the applied stress in the sample to rise or fall) through a feedback loop involving measured axial or radial strain depending on the test configuration.

4.2.1 Axial Strain Controlled Tests

In these tests the target is constant axial strain (maintained by modulating axial force).

4.2.1.1 Multi-step

The decrease in stress relaxation and the change in radial strain for each load level are illustrated in Fig. 6 on the two samples (i.e. Jura_25R and Jura_26R).

Most tests reached linearity, a steady load level, where no further load decrease took place (stress relaxation terminated) within the first 6 hours of testing as shown in Figure 5-6, although most stages were held longer. It was also observed that the relaxation time of each step varied in relation to the initial applied load, as the load increases the relaxation time increased as well.

4.2.1.2 Single-Step

A selection of the relaxation results of Jurassic and Cobourg samples with respect to stress decrease and radial strain are shown in Fig. 7. It should be stated that the Jurassic samples needed less time to reach linearity in terms of stress relaxation than did the Cobourg samples. Considering the data presented in Fig. 7, given that both rock types were subjected to approximately the same initial load, the duration is likely related to the stiffness of the samples. For the same applied load, the axial strain of the Cobourg sample is 0.1% larger than the Jurassic sample. This means that the amount of strain energy stored in the Cobourg sample is greater than that of the Jurassic sample and therefore requires more time to dissipate. The difference in stiffness can be attributed to the argillaceous content of the Cobourg samples (Armstrong and Carter, 2006). It was observed that the samples relaxed within the first hour when subjected to a stress level below CI for both rock types, and as the stress levels approached the CD stress level, the time needed to relax increased relative to the stress increase as was also seen in the multi-step series.

4.2.2 Single-Step vs. Multi-step tests

The multi-step tests showed that the initial stress relaxation was less than the stress reduction observed in the single-step tests at the same load level. It was observed that for the initial load steps in the multi-step tests below CI, shown in Fig. 8, that there was little stress relaxation even for the initial load step (indicated with the light blue lines in Fig. 8). However, when loaded above CI, both the first step of a multi-step test and all single-step tests exhibited stress

relaxation and also showed circumferential deformation, decrease in radial strain with time. This is attributed to the damage evolution within the sample where elastic behaviour governs at load levels below or close to CI and plastic behaviour governs above CI. What is also observed (Fig. 8) is that there is little stress relaxation or change in radial strain for additional steps in the multi-step tests. For this reason, the authors initially considered that the single-step test method should be preferred over the multi-step method when trying to determine the maximum expected relaxation at a given load level.

Time-dependent change in radial strain was observed in some of the relaxation tests as well, where the radial strain decreased initially following the typical trend and once stress relaxation ceased the radial strains began to increase once again; for instance, the behaviour of Jura_26R-g or Jura_25R-e (Fig. 8). The latter was typically observed for the multi-step tests. For both the single and multi-step tests a continued decrease in radial strain was also observed after the stress had relaxed (end of non-linear stress and radial strain changes) and reached linearity; for instance, the behaviour of Jura_30R and Jura_33R shown in Fig. 9.

This has been attributed to a delayed relaxation response and further testing, in combination with creep tests, are required to fully understand the time-dependent mechanisms acting on the sample in this phase of the relaxation test.

This has been attributed to a delayed relaxation response and further testing, in combination with creep tests, are required to fully understand the time-dependent mechanisms acting on the sample in this phase of the relaxation test.

4.3 Radial Strain Controlled Tests

In these tests a target constant radial strain is achieved and maintained by modulating the axial force applied by the piston.

The results of two samples (Jura_02R and Jura_07R) under radial strain-controlled conditions during relaxation are shown in Fig. 10. It was observed that during the first load step the stress increased and no stress relaxation took place. This also occurred for the second step of the multi-step test on Jura_02R (Fig. 10).

It is can be seen from Figure 5-10 that the samples behaviour do not show a uniform behaviour, and is inconsistent with both applied stress levels and time, as stress relaxation is not observed in all stages. It is also inferred that radial strain-controlled conditions provide a small amount of confinement which cannot be quantified and more complex mechanisms take place in these conditions that are closely related to the closure of pre-existing cracks, the initiation, growth and

propagation of new cracks in relation to the feedback oscillation. Under compression, the cracks within the sample tend to open normal to the specimen long axis, but the radial strain is kept constant and as a result the crack growth is prohibited.

The axial stress readings in the radial strain-controlled tests (Fig. 10) fluctuate more than in the axial strain-controlled tests (Fig. 6, 7, 8) because of the feedback delay. This appears to be a small delay in the feedback loop of the servo-machine as the result of the fact that the target constant strain (radial) is perpendicular to the controlling load (axial) and that the mechanistic connection between the radial strain and applied load is less direct than in the axial strain-controlled test. This physical response delay and the resultant control challenges results in more oscillation of the radial strain-controlled test than in an axial strain-controlled test. It was expected that there would be less relaxation under radial strain-controlled conditions as the crack growth is suppressed to some extent but some cracks are allowed to grow because there are small changes in the radial strain occurring as the feedback mechanism requires an oscillation and stress relaxation sometimes takes place, although in an inconsistent manner.

4.4 Effect of Temperature and Humidity

Temperature and humidity changes are known to cause strain of limestone and other rocks (for example: Harvey, 1966; Pimienta et al. 2014). The temperature in the laboratory environment was controlled and both temperature and the humidity were recorded during the testing. The stress and the strain response to temperature and humidity change during an axial strain-controlled single-step test on a sample of Jurassic limestone is presented in Fig. 11. The sample (Jura_28R) presented herein was selected as an example to show the change in the laboratory conditions during relaxation testing does not have a great impact on the material's behaviour with respect to the magnitude of the relaxation.

As a general trend, the changes in both temperature and humidity during tests did not affect the results. This is clearly shown in Fig. 11.b where the change in axial stress and volumetric strain in relation to the change of temperature and humidity is presented. Additionally, it should be stated that temperature and humidity changes showed no general trend and their influence at the measured resolution could be considered negligible as implied from Fig. 11.

The overall change of both temperature and humidity of the tests during the relaxation period is summarized in Table A.2 (see Appendices).

5 ANALYSIS AND DISCUSSION

The examination of the results presented required further analysis in order to investigate closely the rock's response when stress relaxation occurs. It should be noted that the results shown in this section refer to data acquired from axial strain-controlled testing conditions during the relaxation process and do not include the initial loading portion.

5.1 Maximum Stress Relaxation

The initial focus was given to the relation between the maximum stress relaxation in all of the tests; the total change between the maximum stress value at the end of loading and before relaxation started and the lowest stress level resulting after relaxation during the axial strain-controlled tests (holding the axial strain constant) with time. The steps of the procedure undertaken were the following:

- the maximum stress value before relaxation was recorded,
- the initial loading portion of the stress-strain curve was then removed,
- setting the time to zero at the point where the axial strain was kept constant, as illustrated in Fig. 2,
- the load rate was kept the same for all the tests and depending on the instantaneous stress level the initial loading duration ranged from 2 to 20 minutes,
- the axial stress was then normalized to the estimated average UCS, for a better understanding of the results and finally,
- the maximum normalized stress was recorded and related to the maximum stress relaxation (the difference between the initial maximum stress and the minimum stress at the end of the relaxation test where no further relaxation took place).

Each test was analyzed following the above method to determine the maximum stress relaxation. The relations between the maximum stress relaxation and applied stress expressed as a driving ratio of UCS from all the relaxation testing series performed under axial strain-controlled conditions are summarized in Fig.12.a. It can be observed that there is an apparent trend between the multi-step and the single-step tests of Jurassic limestone. Although, they can both fit an exponential relationship between the maximum stress relaxation and the driving stress-ratio, it can be easily seen that for similar driving stress-ratios the multi-step tests exhibit less relaxation than the single-step, as previously discussed.

The mechanism of the initial drop in stress which occurs rapidly for the first step of any test (multi- or single-step) was attributed to be associated with the elastic energy within the sample and load system. Considering this point, a correction procedure was developed to see if the multi-step maximum stress relaxation results could be corrected to the equivalent single-step at the same load level. Since the stress drop was associated with only the initial load stage, this stress drop was added to all subsequent load steps in the multi-step tests, which is shown (Fig. 12.a) as the corrected multi-step series. The corrected multi-step series exhibits similar amounts of stress relaxation compared with the single-step relaxation at a similar load level. Therefore, both single- and multi-step test procedures yield similar trends, when corrected, with increasing driving stress and the multi-step tests can be conducted when limited samples are available. As it has been already discussed, the Cobourg limestone shows a higher relaxation sensitivity as it exhibits more stress relaxation than the Jurassic limestone at the same stress levels.

Note that the stress results shown in Fig.12.a in the horizontal axes were normalized by the peak strength (UCS); however, some samples ended up having values greater than 1 since the average baseline UCS value was used. The results were then normalized to the Crack Initiation threshold (CI), as it was determined from the initial loading part of each relaxation test In Fig.12.b., it is seen that there is an improvement in the fit for the Cobourg samples (higher value of the coefficient of determination R2) when normalizing by CI which is a directly derived value from the tested specimen and not an average value from the UCS testing. However, for the Jurassic limestone the derived CI values from the relaxation tests were more consistent so the R2 values for the fitted curves have similar values. For these reasons, the authors decided to introduce the Crack Initiation Stress-Ratio (CISR) by normalizing the applied stress by the CI value measured on the relaxation sample, where possible, and where loading was below CI the average CI from the baseline UCS testing was taken. Normalization for each relaxation test is shown in Fig.12.b, with the values presented in Table A.3 (see Appendices).

Moreover, the time-dependent behaviour discussed in this paper is interpreted to be, in part, the result of the behaviour of new microcracks, the intensity of which impacts the final UCS value (Diederichs, 2003). Since the loading phase typically went above the CI level, then new microcracks should form, at least during the loading phase. Since the radial strain is decreasing during relaxation, new microcracks are not likely forming or if they are, not in great enough density to result inincreasing the radial strain. It is perhaps possible that existing microcracks are extending, however, future testing could use acoustic emission detection to determine what is happening in terms of new or growth of existing microcracks during relaxation.

5.2 Defining the three stages of stress-relaxation

All the single staged test results showed a similar behaviour during stress relaxation, for both the Jurassic and Cobourg samples. This behaviour can be characterized by three distinct stages, which were observed in the stress relaxation versus time graphs. The three stages from the test results performed on a Jurassic sample under axial strain-controlled conditions are illustrated in Fig. 13. The three stages can also be observed in the radial strain response with time, although there is a slight delay during the transition from stage to stage when compared to the transition time of the stress relaxation shown as dt in Fig. 13 and 14.

The authors define and describe the three stages of stress relaxation in Fig. 14. When the axial deformation is kept constant the stress relaxes with a decreasing rate, this period is defined as the first stage of stress relaxation (R_I). At the end of this stage the stress decrease approaches a constant rate which marks the transition to the second stage (R_{II}). The third stage of relaxation (R_{III}) follows where no further stress relaxation is measureable. At this stage the stress reaches an asymptote and the stress relaxation process is effectively complete, which has been observed by others (for example: Peng, 1973; Rutter, 1978; Hao et al. 2014). It was observed that some samples did not exhibit the second stage of relaxation (R_{II}), as is further discussed in the following sections.

In addition, the radial strain does not always reach an asymptote, even if the stress is constant, when the third stage of stress relaxation is reached. In this case the material is subject to a practically constant axial stress state with ongoing additional absolute radial strain decrease. This response is possibly related to a combination of three-dimensional visco-elastic response and crack behaviour during stable propagation (in the axial direction) under constant axial strain.

5.3 Investigating the three stages of stress relaxation

In this section focus is placed on the material's behaviour during each stage of stress relaxation. The analysis presented examines each stage of relaxation as a percentage of the total behaviour. Each lab testing series is examined and analyzed separately at the beginning and the results are combined after for discussion.

In the following figures, (Fig. 15, 16, 17, 18, 19), the initial applied stress is normalized to the CI value derived from each test, defined previously as the Crack Initiation Stress-Ratio. The stress relaxation (drop) from the applied stress (initial stress-state) for both multi-step and single-step test series for each stage of relaxation are shown in Figure 5-15. The multi-step series (Fig.

15.a) exhibits less relaxation than the single-step for Jurassic limestone (Fig. 15.b). It is clearly seen that the Cobourg limestone (Fig. 15.c) exhibited more stress relaxation as previously discussed. It was also noticed that the Jurassic limestone was subjected to a higher stress level to achieve the same Crack Initiation stress-ratio as with the Cobourg.

The latter could be related to the magnitude of the CI value for each rock type. It is inferred in Fig. 15 that below the elastic limit, both rock formations are exhibiting similar stress relaxation and as the stress level increases the behaviour of the two rock types start to deviate.

During each relaxation stage it was observed that a certain amount of stress relaxation (a percentage of the total stress relaxation, R_T) takes place. The magnitude of the relaxation was examined for each stage of relaxation shown in Fig. 16 as a percentage of the total relaxation.

It can be seen in Fig. 16 that 55% (when the applied stress is closer to CD value) to almost 100% (when the applied stress is below and closer to CI value) of the total stress relaxation (R_T) occurs during the first stage (R_I). While the rest (5% to 45%) of the total stress relaxation takes place during the second (R_{II}) or third stage (R_{III}). There is not always a clear distinction between the two stages (R_{II} and R_{III}) since it was observed that some samples did not exhibit a second stage (R_{II}) and transitioned directly to the third stage (R_{III}) (Fig. 16).

It should be stated here that there is not a clear trend on how the radial strain follows the stress relaxation between the stages in relation to the total radial change, since not all the samples reached a constant value in radial strain and they transitioned into another time-dependent process i.e. creep. In addition, the mechanisms that take place during stress relaxation that lead to displacements and strains are complex, as has been previously found. Fig. 17 shows that the change in radial strain between the stress relaxation stages for the Cobourg limestone does not follow a consistent pattern between the three stages making it difficult for clear conclusions to be derived. As has been discussed, there is a delay in response of the radial strain in relation to the stress relaxation between the three stages. As crack initiation stress-ratio (σ/CI) approaches values of 2.00 which corresponds to the critical damage threshold where crack growth takes place, radial strain cannot be characterized by a clear trend between the three stages of relaxation, as shown in Fig. 17.

The material's response during a relaxation test is summarized in Fig. 18. It illustrates how much time is needed for the stress to relax in relation to the initial applied stress during each stage.

A 5% to 30% stress drop of the initial stress state during 10 to 80% of the total relaxation time occurs during the first stage (R_I), as seen in Fig.18. During the second stage (R_{II}) the stress relaxes less than 10-15% of the initial stress within 20 to 100% of the total relaxation time depending on which the test had reached the third stage and relaxation had been terminated. The third stage (R_{III}) begins at 20% to 80% during which less than 10% relaxation of the initial stress takes place. It is also noticed that the first stage (R_I) has the shortest duration compared to the other two stages (R_{II} and R_{III}) as shown in Fig. 18. It is interpreted from the stress-strain curves during the loading stage that the duration of the first stage (R_I) is influenced by pre-existing damage and to a lesser extent on the accumulated damage dependent on the initial applied stress level.

The relation between the magnitude of stress relaxation occurring in each stage in comparison to the initial applied stress is shown in Figure 5-19. It can be noted that during the first stage (RI) below the CI threshold, approximately 5% to 20% of stress relaxation (comparing to the initial stress) is observed. When the crack initiation stress-ratio is below 0.5, up to 30% of the stress relaxation occurs in the first stage. In this region the presence of pre-existing cracks creates more free surfaces to act as springs and the applied stress is not large enough to completely close or propagate the pre-existing cracks, which could cause increased stress relaxation. During the other two stages (RII and RIII) the stress drops less than 10% of the initial stress. As the applied stress increases the closure of pre-existing cracks takes place and the transition to the plastic behaviour occurs as the initial stress approaches the CD value. To understand this and relaxation behaviour in more detail the laboratory results presented in this paper were compared with existing relaxation testing from the literature.

5.4 Estimating and predicting the relaxation behaviour of rocks

The authors also examined the relationship between standard mechanical properties and the stress relaxation behaviour of the samples tested as part of this research and other rock types reported in the literature. Focus was given to relating both the Crack Initiation Stress-ratio and the elastic Young's Modulus to the maximum stress relaxation and the time period to terminate the relaxation process (i.e. when the stress drop reaches a constant value). The Young's Modulus was normalized to CI and is referred as the Young's Modulus Stress-ratio (E/CI). The selection of the two parameters (CI and Young's Modulus) was made as they can be easily estimated from a relaxation test or from reported values available in literature. The dataset used was primarily focused on the lab results acquired from the relaxation testing on the two different types of limestone (Jurassic and Cobourg) and later was enriched using uniaxial relaxation

testing data on various rock types from previous research as shown in Fig. 3 (Peng and Podnieks, 1972; Peng 1973, Lodus, 1986; Li and Xia, 2000; MODEX, 2002). Knowing the values of either the Young's Modulus or CI, one can estimate the maximum stress relaxation and predict the time that the relaxation is going to occur using the graphs in Fig. 20.

Regarding the data adopted from other researchers presented in Fig. 20 it should be stated that a direct estimation of the CI values from published data was not feasible in all cases. In cases where this was not possible (Peng and Podnieks, 1972; Peng, 1973; Lodus, 1986; Li and Xia, 2000; MODEX, 2002) an estimated value of 40% of the UCS (as per Martin et al. 1999) was used to present the data in a clearer manner.

The trend line shown in Fig. 20.a fits well with the limestone samples tested in this research. However, the rock types showing a higher relaxation potential (e.g. marble, potassium salt, tuff) follow a different trend. The latter is related to the stiffness of the samples as shown in Fig. 20.b. It can be possible then to estimate a rough relaxation behaviour from standard test data. It is recommended that both graphs (Fig. 20.a and b) to be used for estimating the maximum stress relaxation behaviour for a target stress state.

The time needed for the stress to completely relax, is shown Fig. 20.c. It is shown that for some cases (eg. Red sandstone, Arkose sandstone) the time to relaxation decreases as the applied stress increases (initial target stress). This could be attributed to the fact that the stress increase fractures the rock, generating more free surfaces for the stress to relax. The influence of material's stiffness on the relaxation time is shown in Fig. 20.d. It could be inferred that as the material becomes more brittle the stress requires less time to relax. This could explain the fact that the Jurassic limestone needed less time to relax than the Cobourg limestone.

As illustrated in Figure 5-1, stress relaxation tests results, as discussed, can be used to determine parameters used as inputs in numerical simulations for the time-dependent behaviour of brittle rocks assuming that the material behaviour can be phenomenologically simulated as a linear visco-elastic Burgers body. The input parameters are directly related to the values of time-to-relaxation and the magnitude of maximum relaxation (stress drop). These two values are examined in this paper using relaxation test data. In the absence of such data, Fig. 20 can be used to estimate the relaxation behaviour of a material based on conventional mechanical parameters.

Finally, stress relaxation can govern the behaviour of the pillars in mining environments or control the face stability in tunnelling. For instance, the in situ conditions cannot be described

solely by stress-controlled conditions (constant deviatoric stress during creep behaviour) as stress relaxation (strain-controlled conditions) may also occur close to the tunnel face and the overall behaviour of the rock mass can be the result of various time-dependent phenomena in combination. In this regard, this database serves as a first attempt to give more insight into the relaxation behaviour of rocks and could be used by engineers and scientists at the preliminary design stages of underground projects.

CONCLUDING REMARKS (WERE SIMPLIFIED, according to Reviewer #1)

Relaxation is the decrease of applied load at a constant deformation. A relaxation test represents an inversion of the behaviour observed in more common creep testing. This paper evaluates and describes the possible procedures that could be used to conduct a relaxation test.

Relaxation is the decrease of applied load at a constant deformation. A relaxation test represents an inversion of the behaviour observed in more common creep testing. This paper evaluates and describes the possible procedures that could be used to conduct a relaxation test.

It was determined that axial strain-controlled tests provided a more consistent relaxation response and were less sensitive to testing and control challenges.

Single-step tests are practically more convenient but require more samples to obtain the full spectrum of behaviour over the full range of loading magnitudes. Multi-step testing has an advantage in that many data points at different stress levels can be obtained from the same sample. The authors observed that the single-step tests exhibit more stress relaxation and should be preferred to a multi-step test unless the results of the multi-step test are corrected by adding the amount of stress relaxation which occurred in the initial load-stage to each subsequent stage individually.

For either single or multi-step test (axial control), a testing and data analysis procedure has been outlined (Section 5.1) and demonstrated.

For comparison of data from different samples (or different rock types), the maximum relaxation and applied stress levels should be normalized to the crack initiation threshold CI for improved consistency (as compared to UCS).

Load relaxation occurs whenever a crack is initiated, and when stress relaxation attains an asymptotic value, then the stabilization of crack propagation is achieved. The results showed

that the Jurassic limestone relaxes within 6 to 24 hours and the Cobourg limestone needs at least 24 to 48 hours, depending on the stress level the sample is subjected. The samples relaxed within the first hour when subjected to a stress level below CI for both rock types and as the stress level approached the CD stress level the time needed to relax increased relative to the stress increase.

Results of this study demonstrate that there are three distinct stages of time-dependent behaviour observed in relaxation tests based on the standard UCS test configuration for rock. The authors introduced and defined the three stages (R_I, R_{II}, and R_{III}) of stress relaxation. The first two stages are linked to the counterpart stages in the creep test (constant stress). The third stage in the relaxation test presents a very different (inherently stable) behaviour. A comparison of the two testing behaviours is shown in Fig. 21.

Examining the data in detail, it was observed that 55% (when the applied stress is closer to CD value) to almost 100% (when the applied stress is below and closer to CI value) of the total stress relaxation (R_T) occurs during the first stage (R_I). It was also shown that below CI threshold during the first stage (R_I), an approximate of 5% to 20% of stress relaxation (comparing to the initial stress) is expected while for the other two stages (R_{II} and R_{III}) the stress drops less than 10% of the initial stress. Closer to the elastic region, however, it was observed the stress relaxes 30% of the initial stress implying the presence of pre-existence damage in the samples. The closure of the pre-existing cracks takes place with the initial applied stress increase and the transition to the plastic behaviour occurs as the initial stress approaches the CD value.

The study presents a well-defined approach to estimate the maximum stress relaxation and predict the time of the relaxation of various rock formations using the CI value and the Young's Modulus.

This analysis presented herein described the procedure and examined the controlling factors during relaxation testing, discussed the stress relaxation process, defined an analysis method and related the results to previous studies available in the literature and confirmed the existence of the three distinct stages during the relaxation process. Further research is required on the topic to investigate parameters, for instance the change of the rates within the relaxation stages that could better describe the time-dependent behaviour of rocks creating a database that engineers and practitioners could easily use as preliminary tools to both estimate the materials' response and numerically simulate it in complex environments and in-situ conditions where time has a great impact on the rock mass behaviour.

ACKNOWLEDEGMENTS

The authors would like to acknowledge funding for this research from the Nuclear Waste Organization of Canada (NWMO), The Natural Sciences and Engineering Research Council of Canada (NSERC) and the Scientific Equipment Grant Program of ETH Zurich. The assistance of Patric Walter, Julian Felderand, Linus Villiger in sample preparation is greatly appreciated, as well as sample preparation equipment from Professor Jean-Pierre Burg and fruitful discussions with Katrin Wild.

REFERENCES

Armstrong, D.K., and Carter, T.R. 2006. An Updated Guide to the Subsurface Paleozoic Stratigraphy of Southern Ontario. Ontario Geological Survey, *Open File Report 6191*.

ASTM 2013. Standard Test Methods for Stress Relaxation for Materials and Structures. *E328 – 13*.

Aydan, O., Akagi, T., and Kawamoto, T. 1993. The squeezing potential of rocks around tunnels; Theory and prediction. *J. Rock Mech Rock Eng*. **26**(2), pp. 137-63.

Backblom, G,. and Conrox, A.B. 2008. Excvation damage and disturbance in crystalline rock – results from experiments and analyses. *SKB Report TR-08-08*.

Barla, G., 1995. Squeezing rocks in tunnels, *ISRM News Journal*, **3**/**4**, pp. 44-49.

Barla, G., Bonini, M., and Debernardi, D. 2010. Time Dependent Deformations in Squeezing Tunnels. *International Journal of Geoengineering Case Histories*, **2**(1), pp. 819-824.

Bieniawski, T., 1967. Mechanism of Brittle Fracture of Rock, parts I, II, and III. *Rock Mech.MinSci*, **4**(4), pp. 395–430.

Bizjak, K.F., and Zupancic, A., 2007. Rheological investigation for the landslide Slano Blato near Ajdovscina (Slovenia). *Geologija*, **50**(1), pp.121–129.

Brace, W.R., Paulding, B.W.Jr., and Scholz, C. 1966. Dilatancy in the fracture of crystalline rocks. *J. Geophys. Res.*, **71**, 3939-3953, pp. 40-65.

Borchert, K.M., Hebener, H. and Richter, T. 1984. Creep Calculation on salt by using endochronic material law-compared to other creep formulations. The mechanical behaviour of rock salt. *In Proc. of the The Mechanical Behaviour of Rock Salt, edited by H.R. Hardy and M. Langer, Trans Tech Publications*, Clauthal Zellerfeld, W. Germany, pp. 573-587.

Boukharov, G.N., Chanda, M.W., and Boukharov, N.G. 1995. The three processes of brittle crystalline rock creep. *Int. J. Rock Mech. Min Sci. & Geomech*, **32**(4), pp. 325-335.

Brantut N., Heap M.J, Meredith, P.G., and Baud, P. 2013. Time-dependent cracking and brittle creep in crustal rocks: a review. J*. Struct. Geol.*, **52**, pp. 17–43.

Chen, G., and Chugh, Y. 1996. Estimation of in situ visco-elastic parameter of weak floor strata by plate-loading tests. *J. Geotechnical and Geological Engineering*, **14**(2), pp. 151-167.

Damjanac, B., and Fairhurst, C. 2010. Evidence for a long-term strength threshold in crystalline rock. *Rock Mech. Rock Eng.,* **43**(5), pp. 513-531.

Davis, G.H., Reynolds, S.J., and Kluth, CF. 2012. *Structural Geology of Rocks and Regions*, 3rd Edition. Wiley. New York. ISBN:978-1-118-21505-0. 864 pages

Diederichs, M.S., 1999. *Instability of hard rock masses: The role of tensile damage and Relaxation*. Ph.D. Thesis, University of Waterloo, Waterloo, ON, Canada.

Diederichs, M.S. 2003. Rock fracture and collapse under low confinement conditions. *Rock Mech. Rock Eng*. **36** (5), pp. 339-381.

Diederichs, M.S., Kaiser, P.K., and Eberhardt, E. 2004. Damage initiation and propagation in hard rock during tunnelling and the influence of near-face stress rotation. *Int J Rock Mech Min Sci***., 41**(5), pp. 785–812.

Diederichs, M.S. 2007. The 2003 Canadian Geotechnical Colloquium: mechanistic interpretation and practical application of damage and spalling prediction criteria for deep tunnelling. *Can Geotech J*, **44**, pp.1082–1116.

Diederichs, M.S., and Martin, C.D. 2010. Measurement of spalling parameters from laboratory testing. *In: Proc. of Eurock*, Lausanne, Switzerland.

Dunham, J. 1962. *Classification of carbonate rocks according to depositional texture*, pp. 62-84 and 108-121.

Eberhardt, E., Stead, D., Stimpson, B., and Read, R.S. 1998. Identifying crack initiation and propagation thresholds in brittle rock. *Can Geotech J*; **35**, pp. 222-233.

Eberhardt, E., Stimpson, B. and Stead, D. 1999. Effect of grain size on the initiation and propagation thresholds of stress-induced brittle fractures. *Rock Mech. Rock. Eng*. **32**(2), pp. 81-99.

Einstein, H.H. 1996. Tunnelling in difficult ground – swelling behaviour and identification of swelling rocks. *J. Rock Mech. Rock Eng.*, **29** (3), pp. 113-124.

Engelder, T. 1984. The time-dependent strain relaxation of Algerie granite. *Int. J. Rock Mech Min Sci & Geomech*, **2**(2), pp. 63-73.

Fairhurst, C., and Cook, N.G.W., 1966. The phenomenon of rock splitting parallel to the direction of maximum compression in the neighborhood of a surface. *In: Proc. of the First Congress on the International Society of Rock Mechanics*, National Laboratory of Civil Engineering, Lisbon, Portugal, **1**, pp. 687-692.

Fonseka, G.M., Murrell, S.A.F., and Barnes, P. 1985. Scanning electron microscope and acoustic emission studies of crack development in rocks. *Int. J. of Rock Mech. and Min. Sci. and Geomech Abstr.*, **22**(5), pp. 273-289.

Ghaboussi, J., and Gioda, G. 1977. On the time-dependent effects in advancing tunnels. *Int J for Numerical and Analytical Methods in Geomechanics*, **1**, pp. 249-269.

Ghazvnian, E. 2015. *Fracture Initiation and Propagation in Low Porosity Crystalline Rocks: Implications for Excavation Damage Zone (EDZ) Mechanics*, Ph.D. Thesis, Queen' s University, Canada.

Glamheden, R., and Hokmark, H. 2010. *Creep in jointed rock masses*. State of the knowledge. SKB.

Goodman, R. 1980. *Introduction to rock mechanics*. 1st ed. John Wiley and Sons, New York.

Griffith, A.A. 1924. Theory of rupture. *In: Proc of the 1st Int. Congr. Applied Mechanics*, Delft, pp. 55-63.

Groneng, G., Lu, M., Nilsen, B., and Jenssen, A., 2010. Modelling of time-dependent behavior of the basal sliding surface of the Åknes rockslide area in western Norway. *Engineering Geology,* **114**, pp. 414-422.

Hao, S.W., Zhang, B.J., Tian, J.F., and Elsworth, D. 2014. Predicting time-to-failure in rock extrapolated from secondary creep, *J. Geophys. Res. Solid Earth*, **119**, pp.1942–1953.

Harvey, D.R. 1967. *Thermal Expansion of certain Illinois limestones and dolomites*. State of Illinois department of registration and Education, Illinois State Geological Survey, Urbana, Illinois.

Hoek, E., and Brown, T. 1980. *Underground Excavations in Rock*. London: Institution of Mining and Metallurgy, 527 pages.

Hoek, E., Carranza-Torres, C., Diederichs, M.S., and Corkum, B. 2008. *The 2008 Kersten Lecture-Integration of geotechnical and structural design in tunnelling.*

Hoek, E., and Guevara, R. 2009. Overcoming squeezing in the Yacambú-Quibor tunnel, Venezuela. *Rock Mechanics and Rock Engineering*, **42**(2), pp. 389 - 418.

Hudson, J.A., and Harrison, J.P. 1997. *Engineering rock mechanics – an introduction to the principles*. Elsevier, Oxford.

ISRM. 1979. Suggested methods for determining the uniaxial compressive strength and deformability of rock materials.

Lajtai, E.Z. 1974. Brittle failure in compresion. Int. J. of Fracture. **10**(4), pp. 525-536.

Lajtai, E.Z., Duncan, and Carter, J. 1991. The effect of strain rate on rock strength. *Rock Mech. Rock Eng*, **24**, pp.99-109.

Lajtai, E.Z. 1998. Microscopic fracture processes in a granite. *Rock Mech. Rock Eng*. **31**, pp.237-250.

Lau, J.S.O., and Chandler, A. 2004. N.A. Innovative laboratory testing. *Int. J. Rock Mech. Mine Sci*. **41**, pp.1427–1445.

Li, Y., and Xia, C. 2000. Time-dependent tests on intact rocks in uniaxial compression. *Int. J. Rock Mech. Min. Sci*. **37**, pp. 467-475.

Lin, Q. 2006. *Strength Degradation and Damage Micromechanism of Granite under Long-Term Loading,* Ph.D. Thesis, University of Hog-Kong.

Lo, K.Y., and Yuen, C.M.K. 1981. Design of tunnel lining in rock for long term time effects. *Can Geotech. Journal*. **18**, pp. 24-39.

Lockner, D.A., Moore, D.E., and Reches, Z. 1992. *Microcrack intersection leading to fracture.Rock Mechanics*, Rotterdam: Balkema, pp. 807-816.

Lodus, E.V. 1986. *The stressed state and stress relaxation in rocks. Institute of Mining, Academy of Sciences of the USSR*, Leningrad. 2, pp. 3–11.

Malan, D.F., 2002. Simulating the time-dependent behaviour of excavations in hard rock. *Rock Mech. Rock Eng.,* **35**(4), pp. 255-254.

Martin, C.D., Kaiser, P.K., and McCreath, D.R. 1999: Hoek-Brown parameters for predicting the depth of brittle failure around tunnels. *Can. Geotech. J*. **36**(1), pp. 136–151.

Martin, C.D. 1993. *The Strength of massive Lac du Bonnet granite around underground openings*. Ph.D. Thesis. University of Manitoba.

Martin, C.D. 1997. Seventeenth Canadian Geotechnical Colloquium: The effect of cohesion loss and stress path on brittle rock strength. *Can. Geotech. J*. **34**(5), pp. 698–725.

Martin, D., Chandler, A. 1994: The progressive fracture of Lac du Bonnet granite. *Rock Mech. Min. Sci. Geo.* **31**(6), pp. 643-659.

MODEX-REP. 2002. *Experimental Study of the Hydromechanical behaviour of the Callovo-Oxfordian Argillites*.

Nicksiar, M., and Martin, C.D. 2012. Evaluation of methods for determining crack initiation in compression tests on low-porosity rocks. *Rock Mech Rock Eng*, **45**(4), pp. 607–617

Ottosen, N.S. 1986. Visco-elastic-viscoplastic formulas for analysis in rock salt cavities. Inter *Journal Rock Mech. Min. Struct. & Geomech Abstr*. **23**(3). pp. 201-212.

Paraskevopoulou, C., Benardos, A. 2013. Assessing the construction cost of tunnel projects. *Tunnelling and Underground Space Technology*, **38**, pp. 497–505.

Pellet, F., Hajdu, A., Deleruyelle, F., Bensus, F., 2005. A visco-plastic model including anisotropic damage for the time-dependent behaviour of rock. *Int. J. for Numer. Anal. Meth. Geomech*. **29**, pp. 941-970.

Peng, S.S. 1973. Relaxation and the behaviour of failed rock. *Int. J. Rock Mech Min. Sci. & Geomech*. **10**, pp. 235-246.

Peng, S., and Podnieks E.R. 1972. Relaxation and the behaviour of failed rock. *Int, J. Rock Mech. Min. Sci*., **9**, pp. 699-712.

Pimienta, L., Fortin, J., and Gueguen, Y., 2014. Investigation of elastic weakening in limestone and sandstone samples from moisture adsorption. *Geophys. J. Int*., **199**, pp. 335-347.

Podnieks E.R., Chamberlain, P.G., and Thill R.E.1968. Environmental Effects on Rock Properties, *In: Proc. of the Tenth Symposium of Rock Mechanics*, University of Missouri at Rolla.

Potyondy, D. 2007. Simulating stress corrosion with a bonded-particle model for rock. *Int, J. Rock Mech. Min. Sci*. **44**, pp. 677-693.

Rutter, E.H., Atkinson, B.K., and Mainprice, D.H. 1978. On the use of stress relaxation testing method in studies of the mechanical behaviour of geological materials. *Geophys. J. R. Astr. Soc.*, **55**, pp. 155-170.

Schmidtke, H., and Lajtai, E.Z. 1985. The long term strength of Lac du Bonnet granite. *Rock Mech. Min. Sci. Geo.,* **22**, pp. 461–465.

Scholz, C.H. 1968. Mechanism of creep in brittle rock. *J of Geophysical Research*, **73**(10), pp. 3295-3302.

Schubert, W., Button, E.A., Sellner P.J., and Solak, T. 2003. Analysis of time-dependent displacements of tunnels. *J. Rock Mechanics*, **21**(5), pp. 96-103.

Singh, D.P. 1975. A study of creep of rocks. Int. J. Rock Mech Sci & Geomech, **12**, pp. 271-276.

Sterling, S., Jackson, R., Walsh, R., Heagle, D., and Clark, I. 2011. Assessment of porosity data and gas phase presence in DGR cores. NWMO Technical Report, *TR-08-34*.

Wawesik, W.R. 1972. Time-dependent rock behaviour in uniaxial compression. *In: Proc. of the 14th Rock Mechanics Symposium*, University of Pennsylvania, pp. 85-106.

Zheng, S.F., and Weng, G.J. 2002. A new constitutive equation for the long-term creep of polymers based on physical aging. *European J. of Mechanics A/Solids,* **21**, pp. 411-421.

Table I. Summary of the relaxation testing types. For each multi-step test, 10 strain levels were tested.

Rock Formation	**Jurassic** limestone				**Cobourg** limestone			
Type of Test	Axial-controlled		Radial-controlled		Axial-controlled		Radial-controlled	
Load Level(s)	Single-step	Multi-step	Single-step	Multi-step	Single-step	Multi-step	Single-step	Multi-step
Number of Samples	14	2	--	3	16	--	--	--
Total	19				16			

Table A.1. Results from Baseline testing for a. Jurassic limestone and b. Cobourg limestone

a. Values for Jurassic limestone						b. Values for Cobourg limestone					
Sample Name	UCS (MPa)	CD (MPa)	CI (MPa)	E* (GPa)	Poisson's ratio*	Sample Name	UCS (MPa)	CD (MPa)	CI (MPa)	E* (GPa)	Poisson's ratio*
JURA_1U	66	53	27	103	0.26	CBRG_1U	104	93	45	38	0.24
JURA_2U	114	89	40	73	0.12	CBRG_3U	146	132	56	37	0.18
JURA_3U	88	74	36	125	0.29	CBRG_4U	122	111	44	45	0.17
JURA_4U	112	100	46	86	0.26	CBRG_5U	136	110	52	47	0.16
JURA_5U	126	102	45	101	0.29	CBRG_6U	132	113	52	46	0.15
JURA_6U	101	97	35	71	0.18	CBRG_7U	107	96	47	36	0.13
JURA_7U	68	64	22	95	0.22	CBRG_8U	94	84	37	37	0.12
JURA_8U	137	125	50	89	0.25	CBRG_9U	149	136	58	41	0.11
JURA_9U	110	105	42	94	0.21	CBRG_10U	136	124	56	44	0.13
JURA_10U	111	99	44	92	0.22						
Avg.	103	91	39	93	0.23		125	111	50	41	0.15
St. Dev.	23	21	9	15	0.05		19	18	7	4	0.04

**The elastic parameters were derived from the linear portion of the complete stress-strain curves.*

Table A.2. Change in Temperature and Relative Humidity during relaxation time.

Multi-step			
Jura_Axial-Controlled			
Sample Name	Temp (°C)	RH (%)	Relaxation Time (Sec)
JURA_25R-a	-1.5	--	6994.4
JURA_25R-b	0.5	--	34751.0
JURA_25R-c	-0.5	--	48830.4
JURA_25R-d	0.0	--	81246.8
JURA_25R-e	-0.2	--	44087.0
JURA_25R-f	0.2	--	42884.7
JURA_25R-g	-0.5	--	42617.5
JURA_25R-h	0.3	--	42775.1
JURA_25R-i	-0.3	--	83618.9
JURA_25R-j	0.0	--	4320.8
JURA_26R-a	0.0	--	20987.1
JURA_26R-b	-0.2	--	72472.4
JURA_26R-c	0.2	--	80521.4
JURA_26R-d	-0.1	--	77386.0
JURA_26R-e	-0.3	--	35372.5
JURA_26R-f	0.2	--	50234.3
JURA_26R-g	-0.1	--	91664.0
JURA_26R-h	-0.2	--	29330.4
JURA_26R-i	0.2	--	18401.0
JURA_26R-j	-0.1	--	86307.9
Radial-Controlled			
Sample #	Temp	RH	Relaxation Time
JURA_07R-a	1.0	--	52459.6
JURA_07R-b	0.5	--	23029.4

Single-step			
Jura_Axial-Controlled			
Sample Name	Temp (°C)	RH (%)	Relaxation Time (Sec)
JURA_27R	-0.2	0.1	5804.1
JURA_28R	-0.4	2.7	37865.3
JURA_29R	0.1	1.0	51576.5
JURA_30R	-0.7	0.3	22967.5
JURA_31R	0.0	-2.3	60987.6
JURA_32R	-0.4	-0.8	76535.4
JURA_33R	--	--	85140.5
JURA_34R	-3.5	12.8	75077.8
JURA_35R	-0.1	1.5	52523.4
JURA_36R	-0.7	-1.2	270393.1
JURA_39R	-4.3	5.2	83222.4
JURA_40R	-0.7	5.7	89768.6
JURA_41R	-0.7	-2.8	85947.9
JURA_44R	4.4	3.3	70913.501
Cobourg_Axial-Controlled			
Sample #	Temp	RH	Relaxation Time
CBRG_16R	-2.7	-3.1	67726.2
CBRG_16R-b**	-0.7	-2.5	50240.7
CBRG_17R	0.2	-4.6	5791.9
CBRG_17R-b**	--	--	161120.6
CBRG_18R	-0.1	7.8	69133.5
CBRG_18R-b**	--	--	*No relaxation data*
CBRG_19R	-0.2	-8.6	86046.5
CBRG_20R	-0.3	5.6	73728.8
CBRG_21R	--	--	73784.0
CBRG_22R	0.6	--	132077.0
CBRG_23R	-0.3	--	131298.9
CBRG_24R	-1.5	--	79790.7
CBRG_25R	-2.7	--	193521.5
CBRG_26R	-1.8	31.7	247858.8
CBRG_27R	0.3	-4.4	83728.8
CBRG_28R	-4.2	5.8	251275.4
CBRG_29R	-3.3	-2.9	151099.8
CBRG_30R	-1.2	5.2	152054.9

***these samples were tested again to a higher stress level*

(-) refers to increase and (+) to decrease

Table A.3. Summary of elastic and mechanical properties estimated from Relaxation testing.

a. Values for Jurassic limestone

Sample #	CI (MPa)_LL - Martin & Chandler 1994	CI (MPa)_UL -Martin & Chandler 1994	CI (MPa) - Lajtai_1974	E (GPa)	Poisson's ratio	Driving Stress-ratio (σ/UCS)
JURA_27R	25	34	42	53	0.19	0.51
JURA_28R	25	32	43	55	0.17	0.61
JURA_29R	37	38	48	57	0.16	0.75
JURA_30R	28	40	47	60	0.18	0.88
JURA_31R	21	33	48	57	0.20	0.98
JURA_32R	30	37	48	63	0.15	0.57
JURA_33R	25	33	41	63	0.11	0.46
JURA_34R	22	35	44	58	0.15	0.80
JURA_35R	25	37	45	55	0.16	0.84
JURA_36R	20	36	45	54	0.16	0.95
JURA_39R	--	--	--	59	0.17	0.09
JURA_40R	--	--	--	52	0.12	0.08
JURA_41R	--	--	--	56	0.13	0.09
JURA_25R-a*	--	--	--	54	0.15	0.09
JURA_26R-a*	28	33	42	55	0.14	0.42

b. Values for Cobourg limestone

Sample #	CI (MPa)_LL - Martin & Chandler 1994	CI (MPa)_UL -Martin & Chandler 1994	CI (MPa) - Lajtai_1974	E (GPa)	Poisson's ratio	Driving Stress-ratio (σ/UCS)
CBRG_16R	10	13	20	31	0.09	0.28
CBRG_16R-b**	15	33	35	37	0.09	0.35
CBRG_17R	20	31	37	38	0.15	0.35
CBRG_17R-b**	22	47	45	41	0.16	0.69
CBRG_18R	17	33	36	38	0.12	0.43
CBRG_18R-b**	14	34	41	37	0.09	0.64
CBRG_19R	20	28	33	38	0.12	0.47
CBRG_20R	18	28	34	36	0.13	0.50
CBRG_21R	20	39	39	38	0.11	0.59
CBRG_22R	22	35	33	29	0.09	0.50
CBRG_23R	15	28	32	29	0.12	0.52
CBRG_24R	15	23	34	27	0.07	0.49
CBRG_25R	12	32	37	32	0.13	0.59
CBRG_26R	15	43	42	34	0.17	0.75
CBRG_27R	19	28	40	34	0.13	0.76
CBRG_28R	16	42	45	33	0.13	0.75
CBRG_29R	20	27	32	27	0.12	0.50
CBRG_30R	--	--	--	25	0.08	0.09

**the first stage of the multi-step tests*

***these samples were tested again to a higher stress level*

LIST OF FIGURES

Figure 10. Radial-strain-controlled multi-step relaxation results of two Jurassic samples (Jura_02R and Jura_07R). Axial stress (blue line), axial strain (brown line) and radial strain (red line) results in relation to relaxation time expressed in seconds. The damage thresholds of CI and CD refer to the average values derived from the UCS baseline tests.

Figure 11. a.) Axial stress response of Jura_28R sample to temperature and relative humidity fluctuations during relaxation testing and b.) Volumetric strain response of Jura_28R sample to temperature and relative humidity fluctuations during relaxation testing.

Figure 12. a.) Maximum Stress–Relaxation (MPa) to Driving Stress-Ratio normalized to UCS and b.) Maximum Stress – Relaxation (MPa) to Crack Initiation Stress-Ratio CISR (applied initial stress normalized to CI) of the single-step tests on the Jurassic (in blue) and Cobourg (in red) samples, as well as the multi-step tests of the Jurassic samples (in green). 'Ax' refers to axial-strain-controlled conditions and 'ss' and 'ms' denotes single-step load and multi-step load tests, respectively.

Figure 13. The three stages of the stress-relaxation process during a relaxation test under axial-strain-controlled conditions illustrated on the Jura_33R sample.

Figure 14. The three stages of the stress-relaxation process during a relaxation test under axial-strain-strain controlled conditions.

Figure 15. Axial stress relaxation (drop) in relation to the Crack Initiation Stress-ratio (normalized to CI from the testing series) for Jurassic limestone (a. and b.) and Cobourg limestone (c.). 'Ax' refers to axial-strain-controlled conditions, 'ms' and 'ss' denotes the multi-step and single-step load series, respectively. R-0, R-I, R-II and R-III refer to the initial state, the first, the second and the third stage of relaxation, respectively.

Figure 16. Percentage of stress relaxation during each relaxation stage in relation to the Crack Initiation Stress-ratio (normalized to CI from the testing series) for Jurassic limestone (a. and b.) and Cobourg limestone (c.). 'Ax' refers to axial-strain-controlled conditions, 'ms' and 'ss' denotes the multi-step and single-step load series, respectively. R-0, R-I, R-II and R-III refer to the initial state, the first, the second and the third stage of relaxation, respectively.

Figure 17. Percentage of total change in radial response during each relaxation stage in relation to the Crack Initiation Stress-ratio (normalized to CI from the testing series) for Cobourg limestone. 'Ax' refers to axial-strain-controlled conditions and 'ss' denotes single-step load series. R-0, R-I, R-II and R-III refer to the initial state, the first, the second and the third stage of relaxation, respectively.

Figure 18. Percentage of stress relaxation to the initial (applied) stress in relation to the percentage of relaxation time during each relaxation stage testing series for Jurassic limestone and Cobourg limestone. 'Ax' refers to axial-strain-controlled conditions and 'ss' denotes the single-step load series. R-0, R-I, R-II and R-III refer to the initial state, the first, the second and the third stage of relaxation, respectively.

Figure 19. Percentage of stress relaxation to the initial (applied) stress during each relaxation stage in relation to the to the Crack Initiation Stress-ratio (normalized to CI from the testing series) for Jurassic limestone (a.) and Cobourg limestone (b.). 'Ax' refers to axial-strain-controlled conditions and 'ss' denotes the single-step load series. R-0, R-I, R-II and R-III refer to the initial state, the first, the second and the third stage of relaxation, respectively.

LIST OF TABLES

Fig. 1

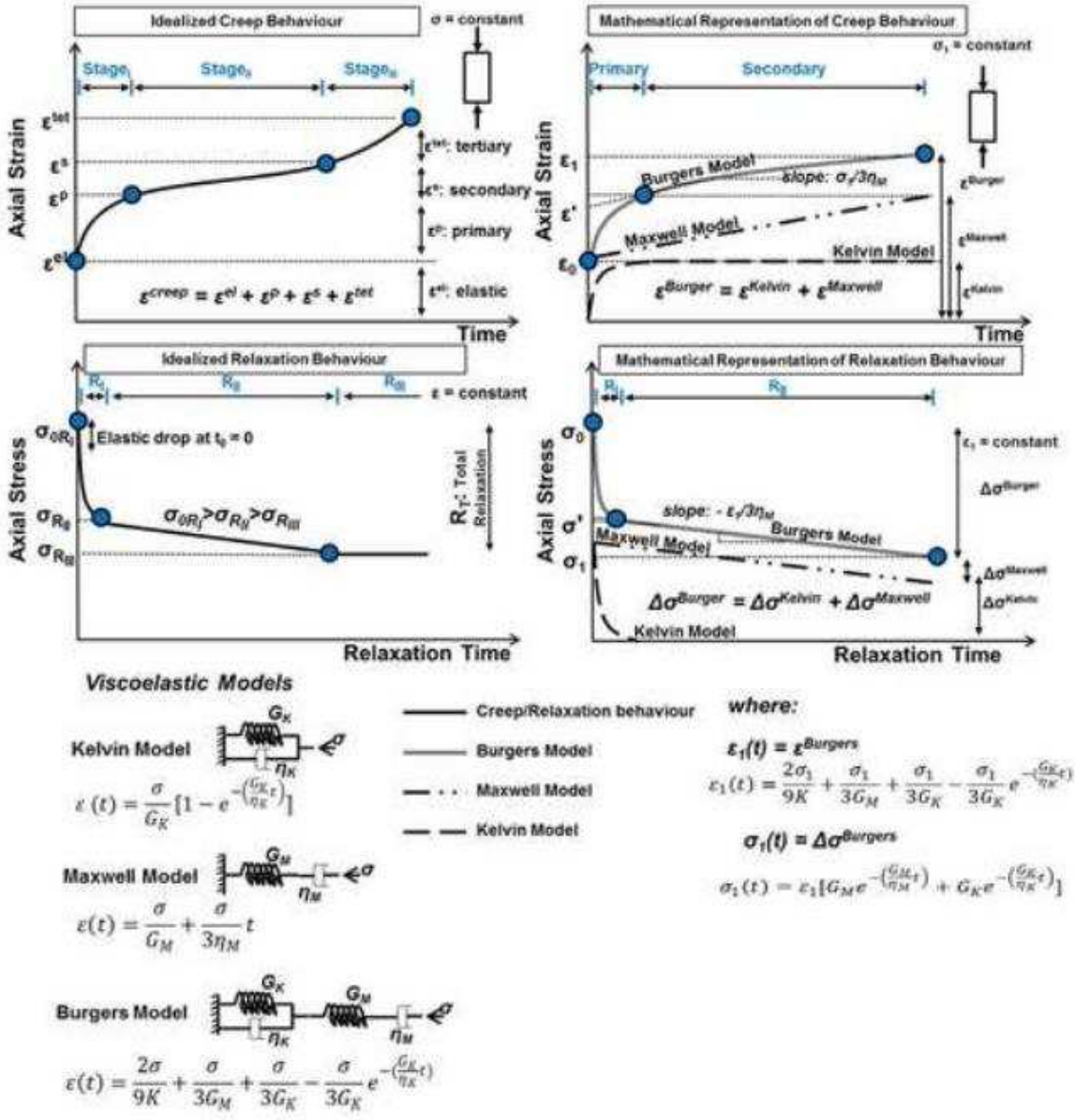

$$\varepsilon(t) = \frac{\sigma}{G_K}\left[1 - e^{-\left(\frac{G_K}{\eta_K}t\right)}\right]$$

$$\varepsilon(t) = \frac{\sigma}{G_M} + \frac{\sigma}{3\eta_M}t$$

$$\varepsilon(t) = \frac{2\sigma}{9K} + \frac{\sigma}{3G_M} + \frac{\sigma}{3G_K} - \frac{\sigma}{3G_K}e^{-\left(\frac{G_K}{\eta_K}t\right)}$$

$$\varepsilon_1(t) = \frac{2\sigma_1}{9K} + \frac{\sigma_1}{3G_M} + \frac{\sigma_1}{3G_K} - \frac{\sigma_1}{3G_K}e^{-\left(\frac{G_K}{\eta_K}t\right)}$$

$$\sigma_1(t) = \varepsilon_1\left[G_M e^{-\left(\frac{G_M}{\eta_M}t\right)} + G_K e^{-\left(\frac{G_K}{\eta_K}t\right)}\right]$$

Fig. 2

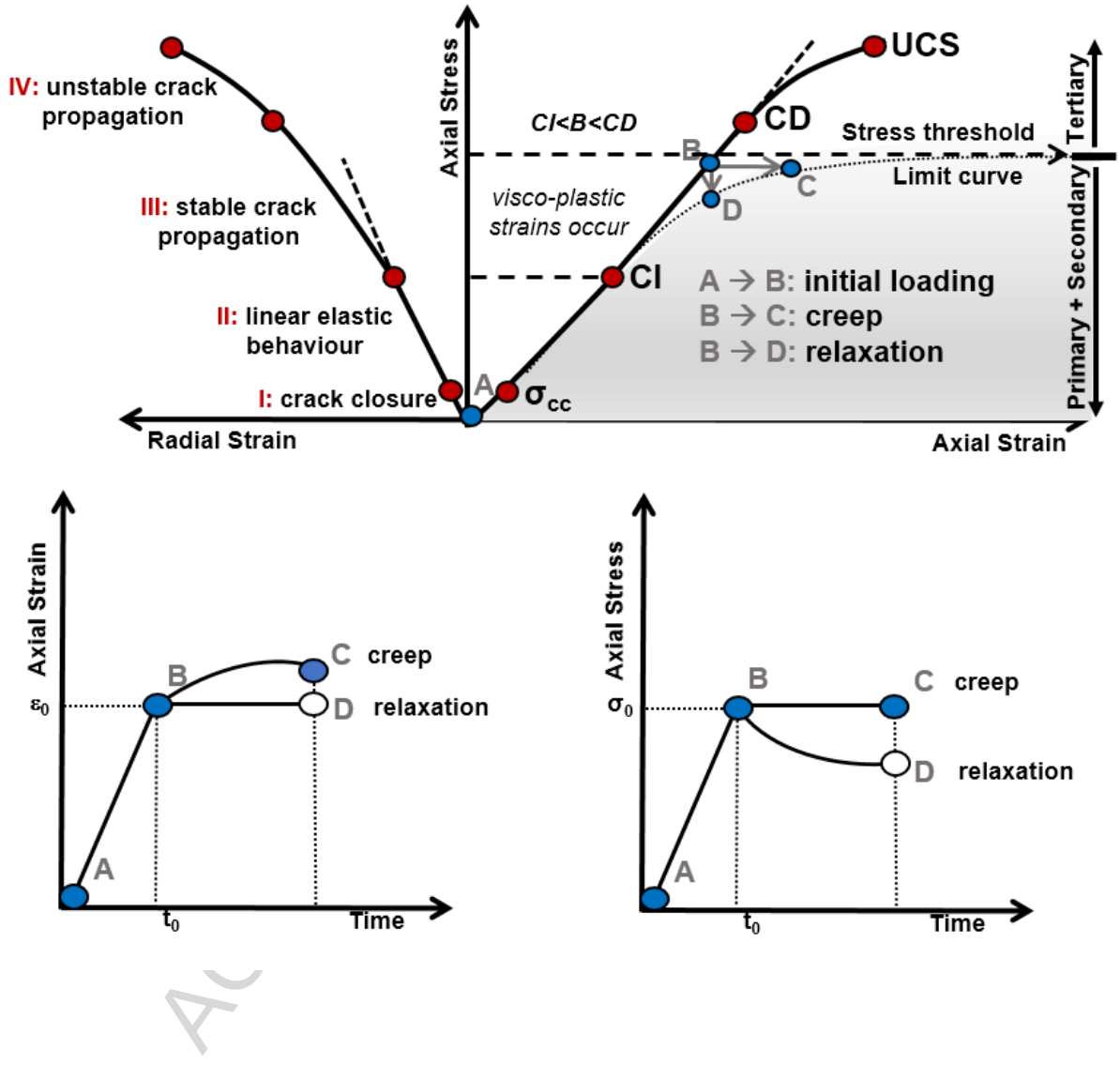

Fig. 3

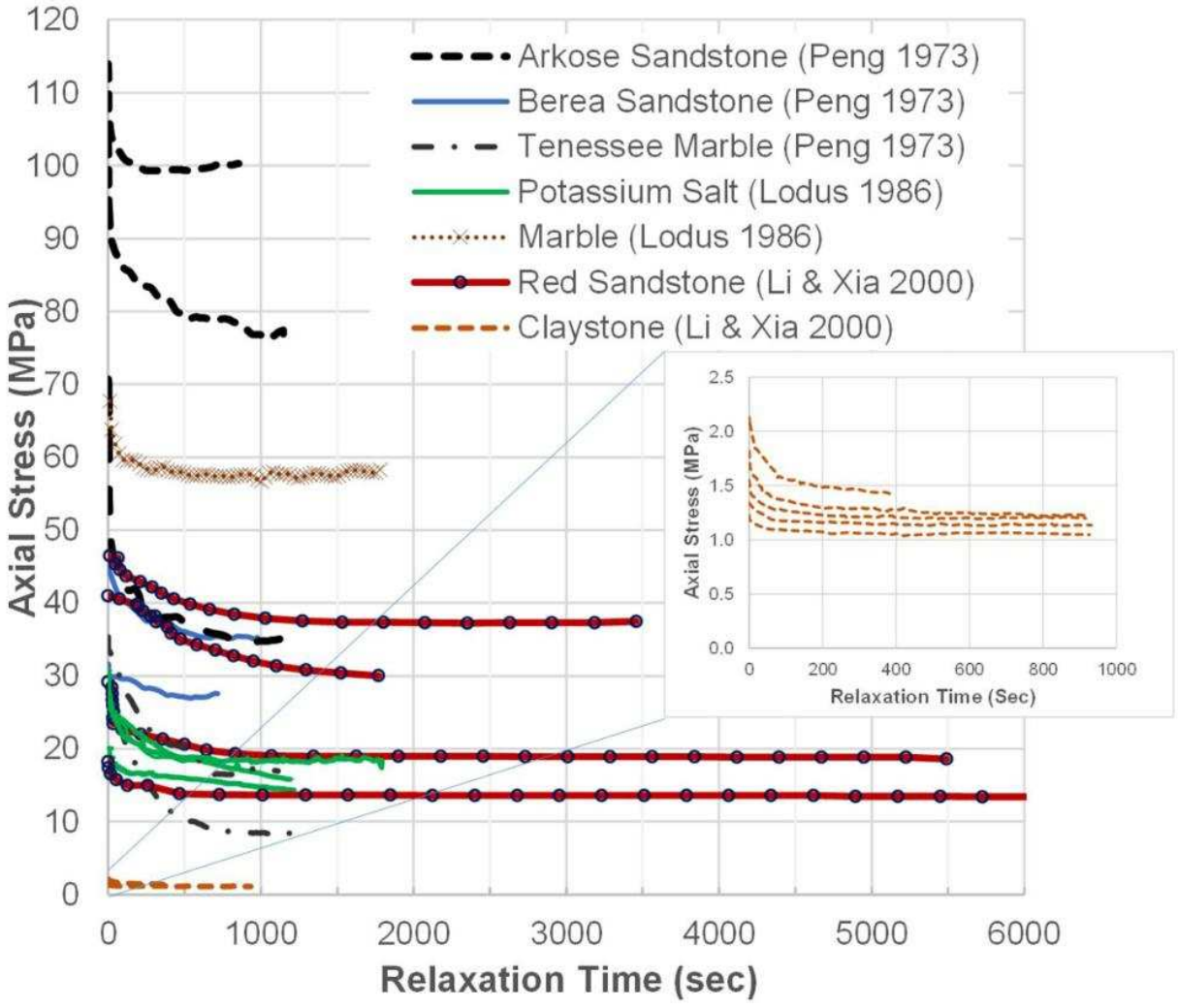

Fig. 4

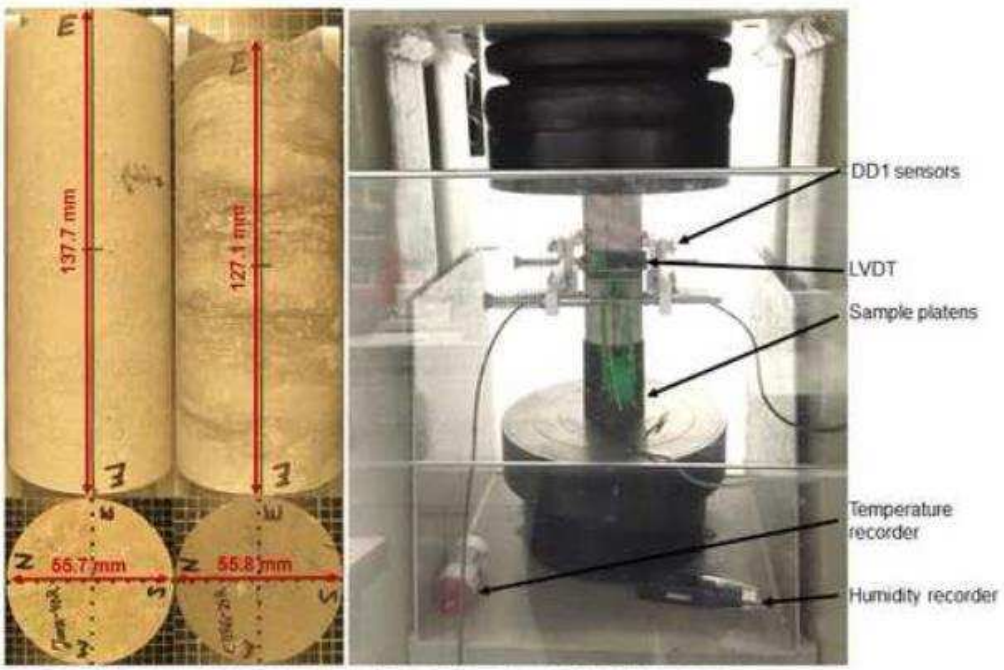

a. Jura b. Cobourg c. Equipment of stress relaxation testing

Fig. 5

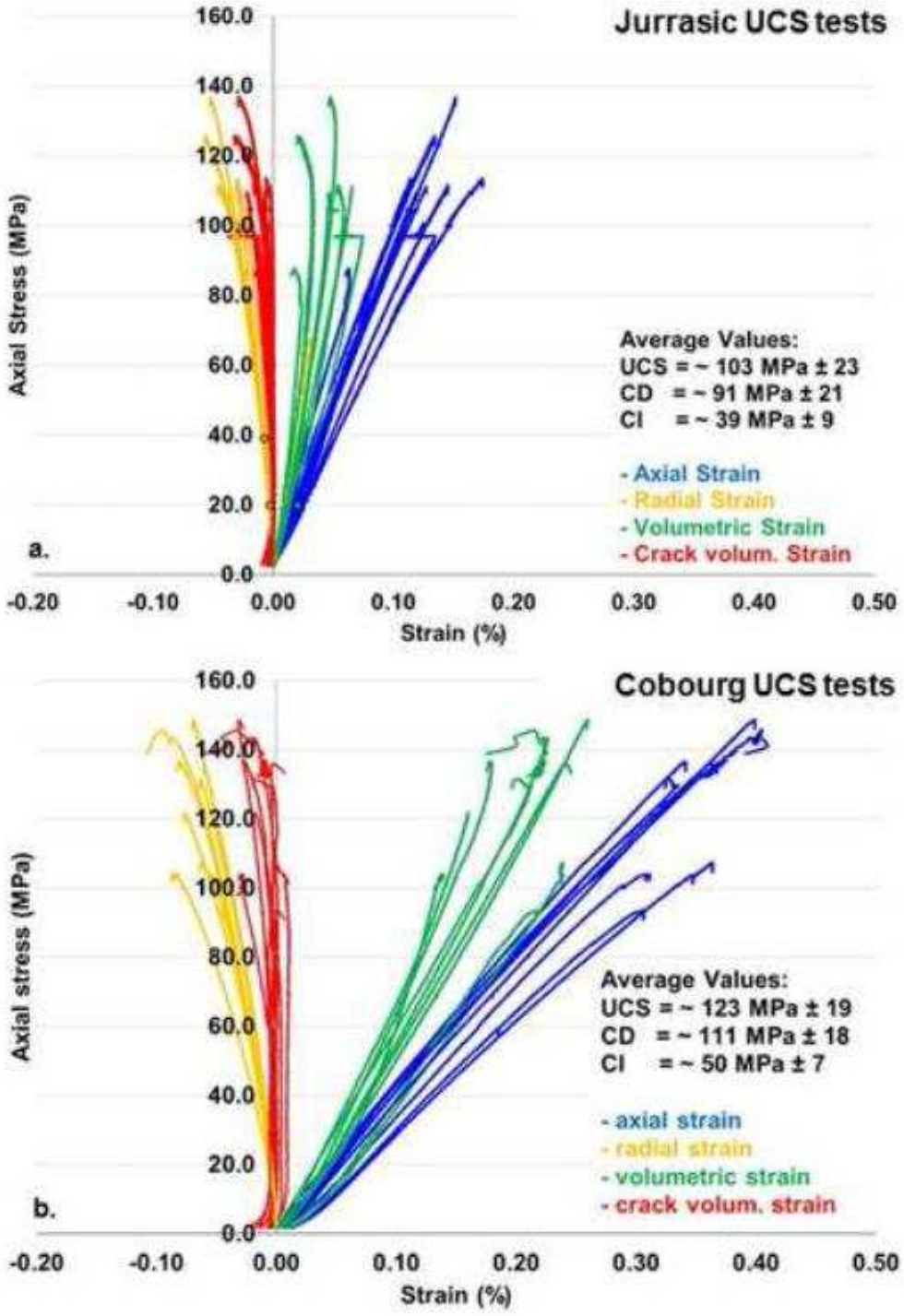

Fig. 6

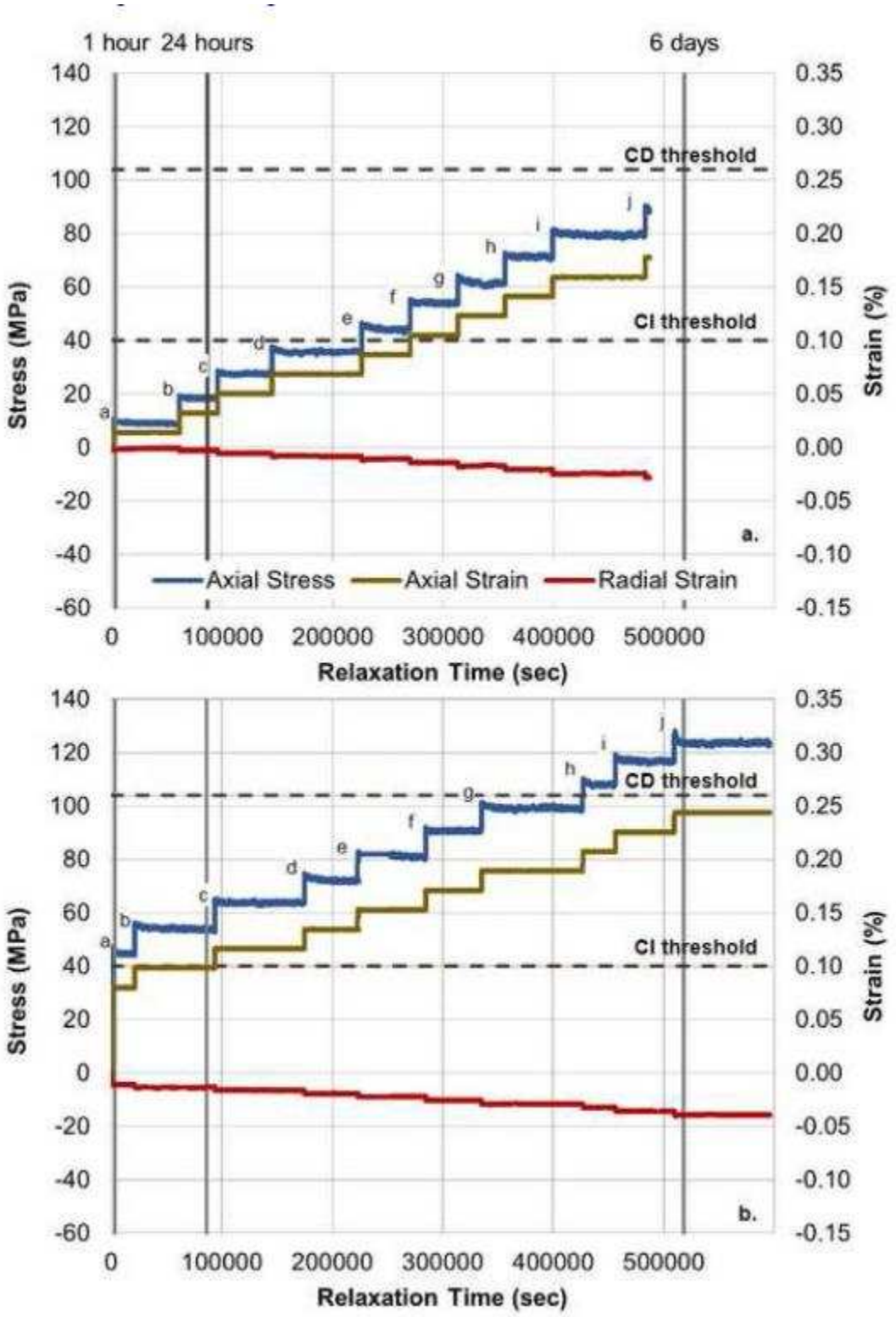

Fig. 7

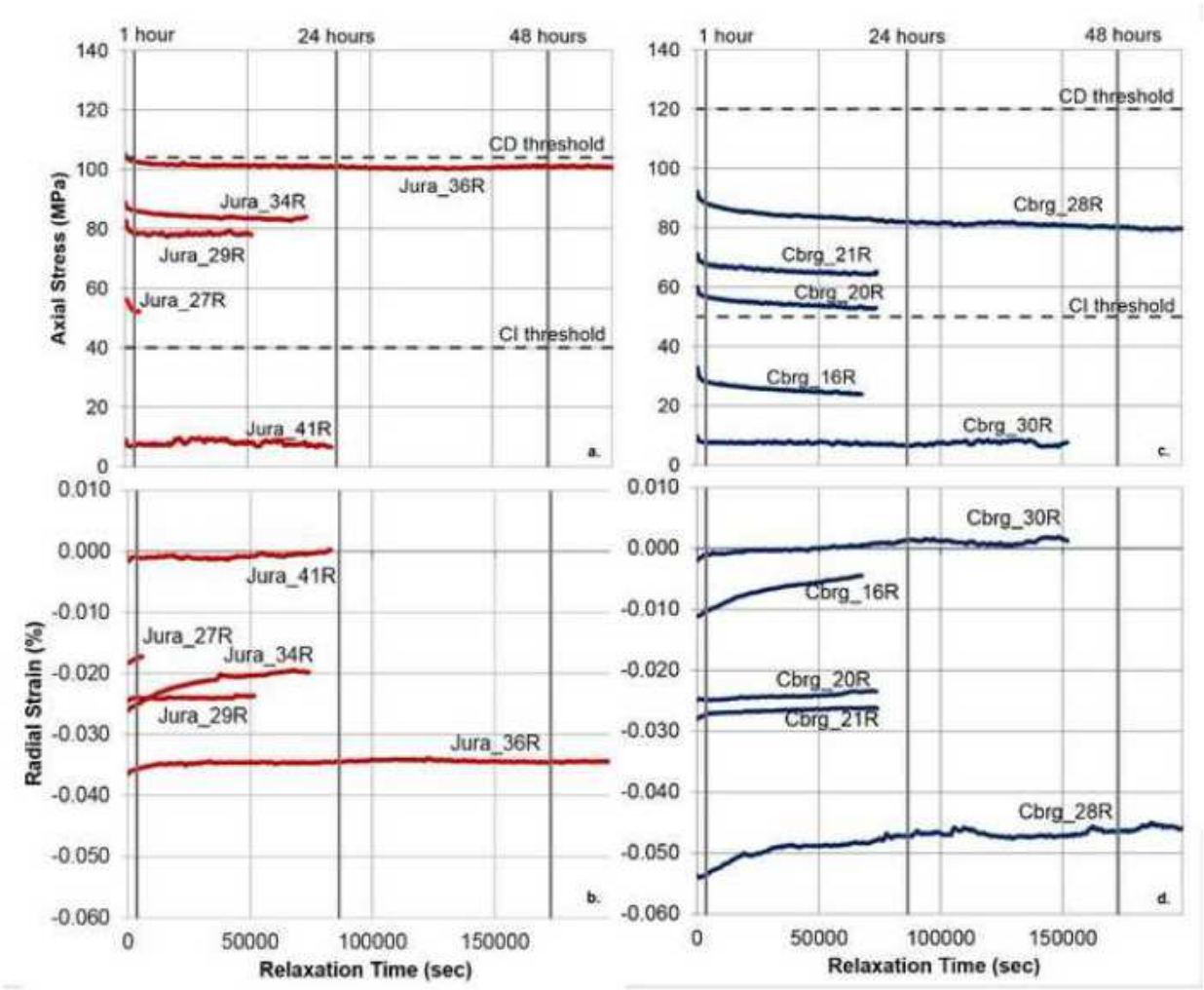

Fig. 8

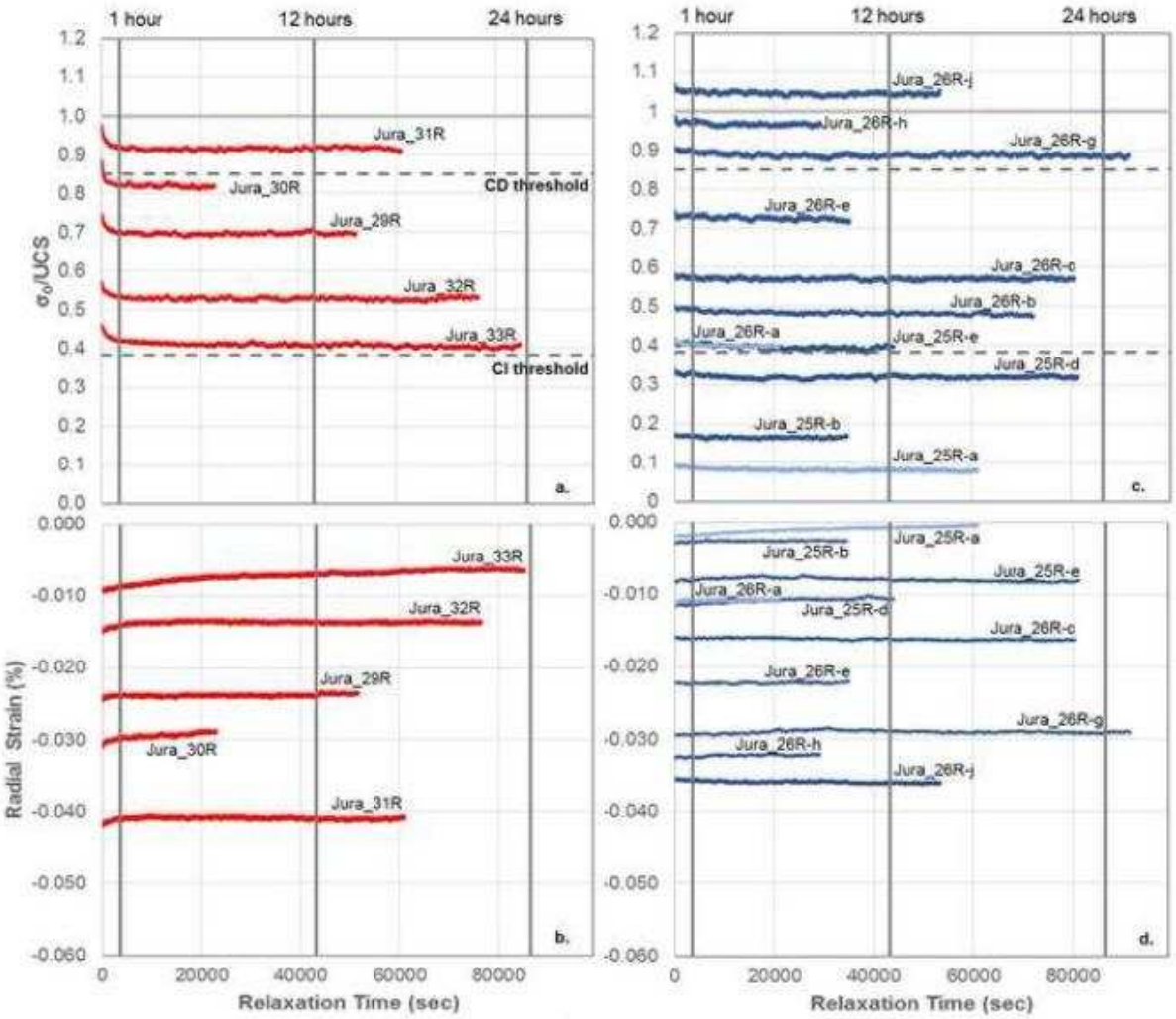

Fig. 9

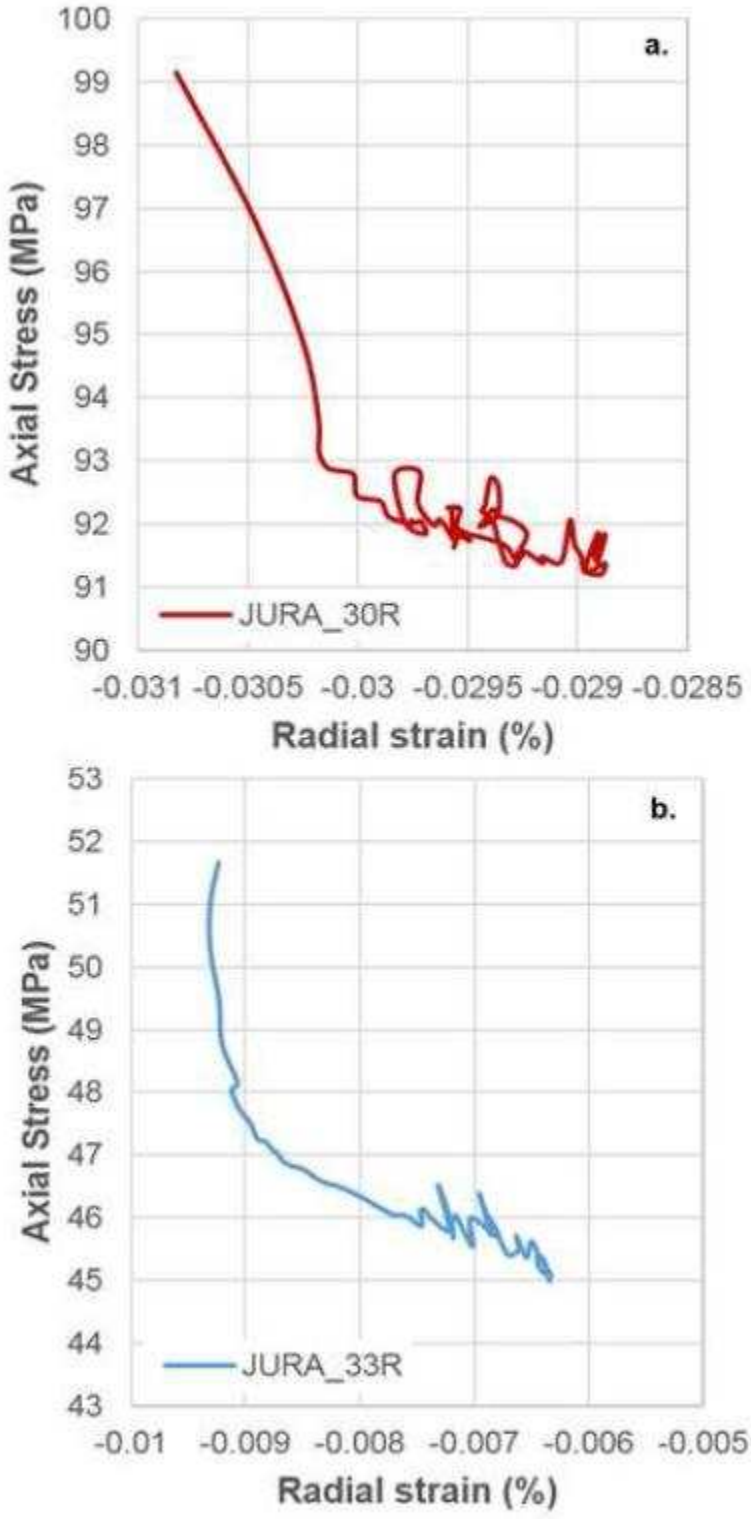

Fig. 10

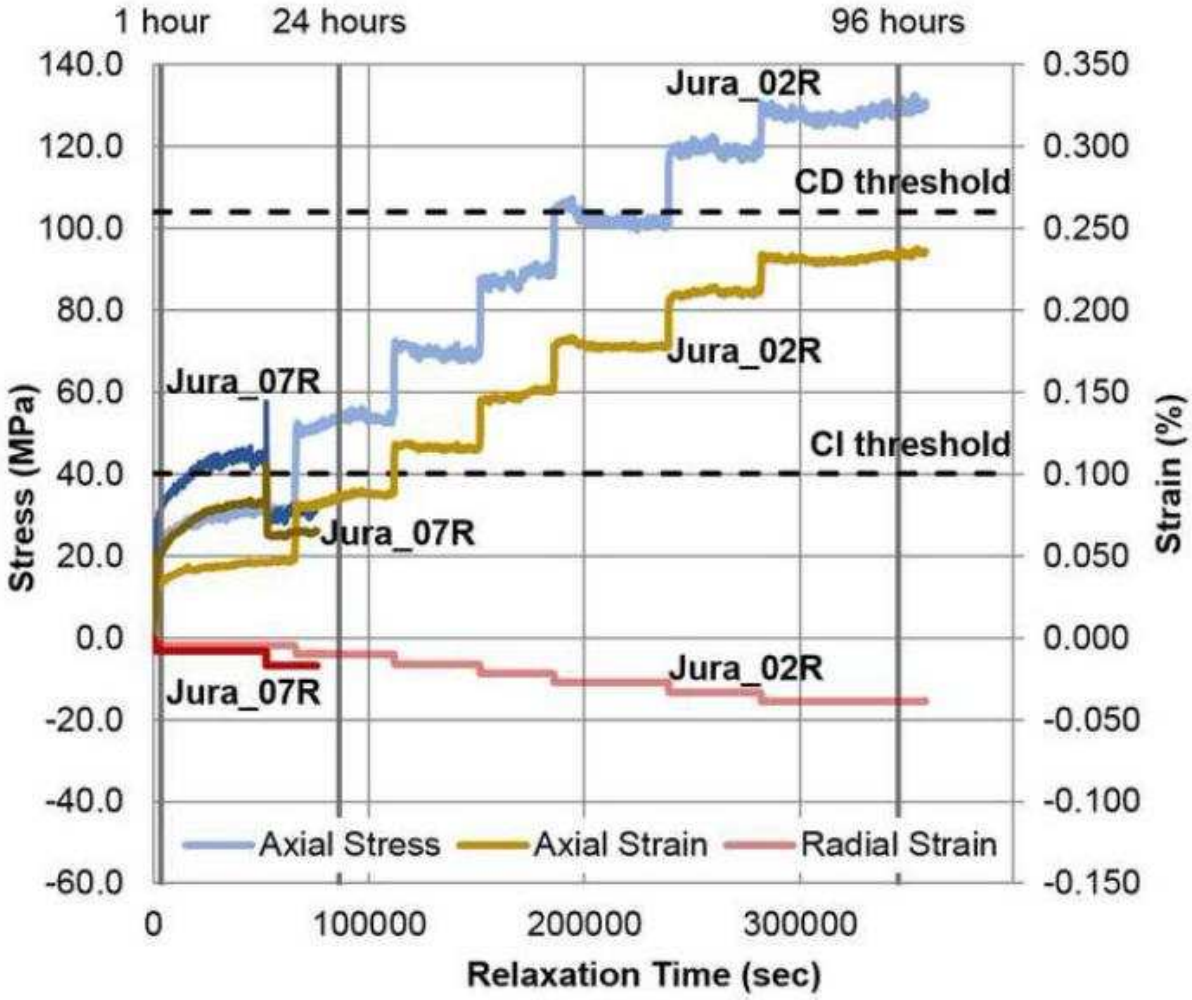

Fig. 11

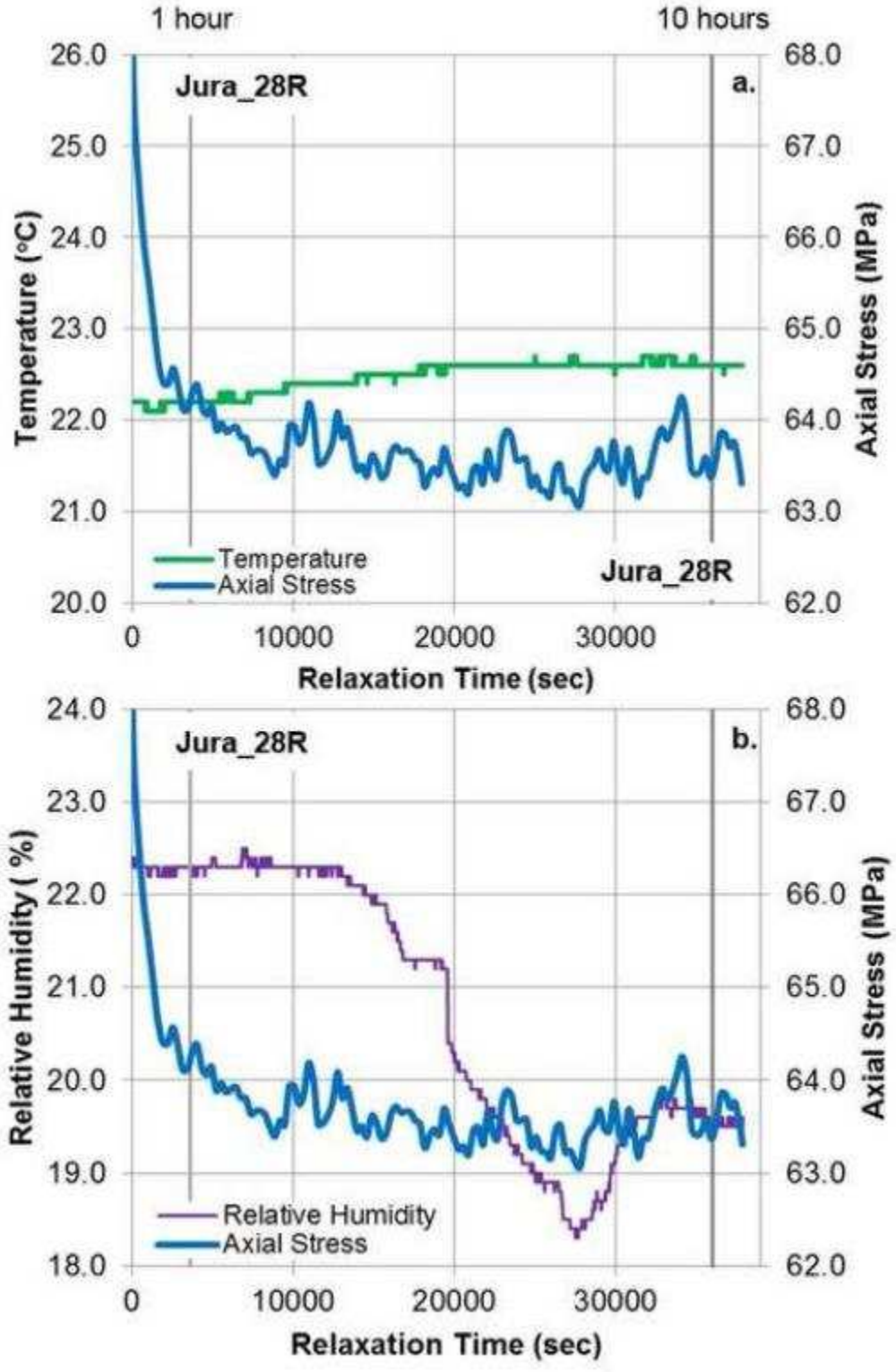

Fig. 12

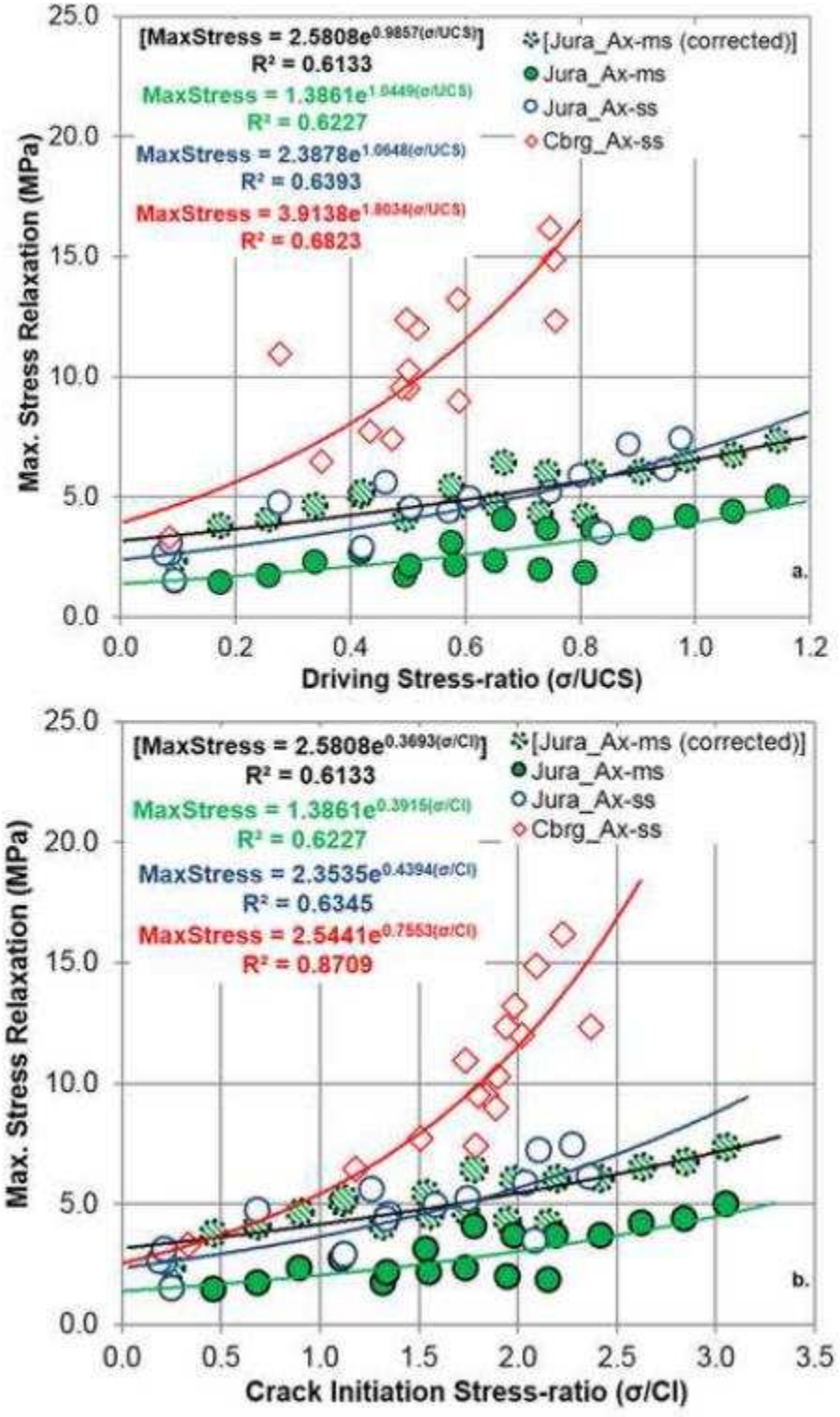

Fig. 13

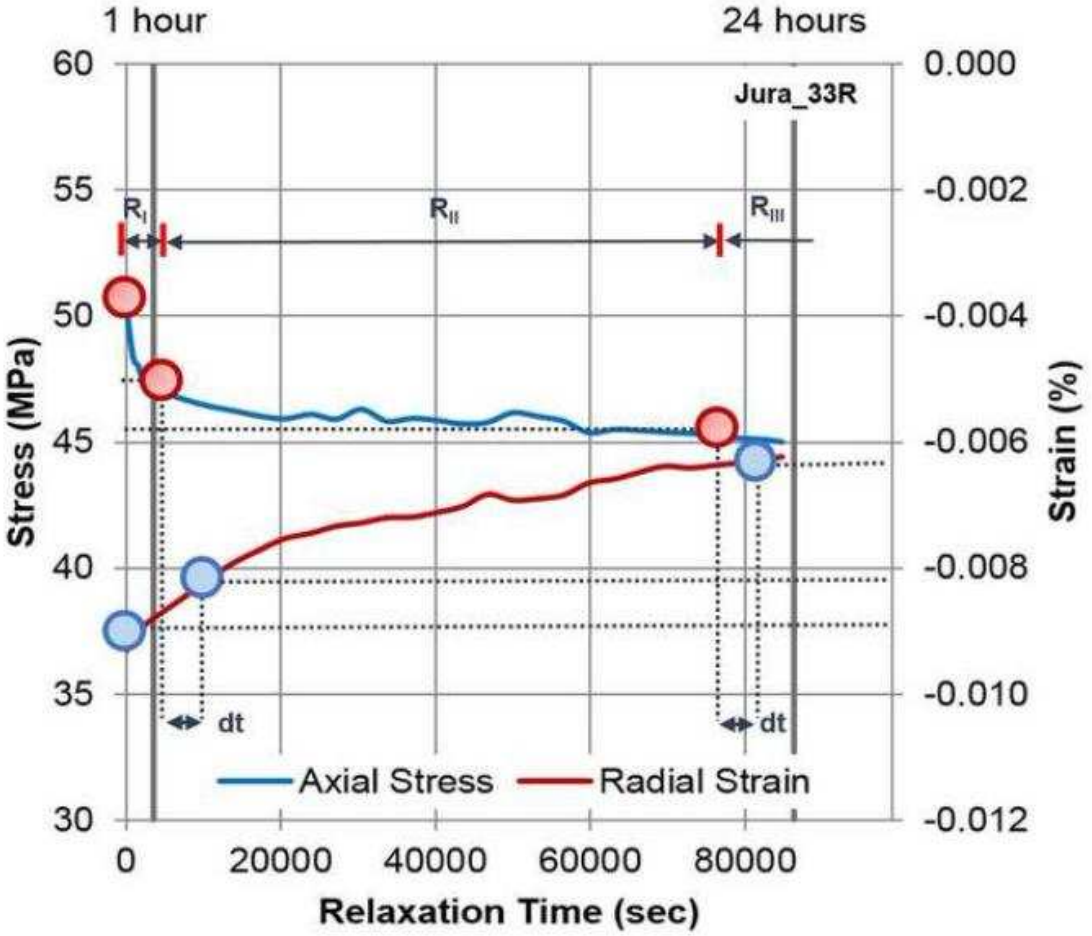

Fig. 14

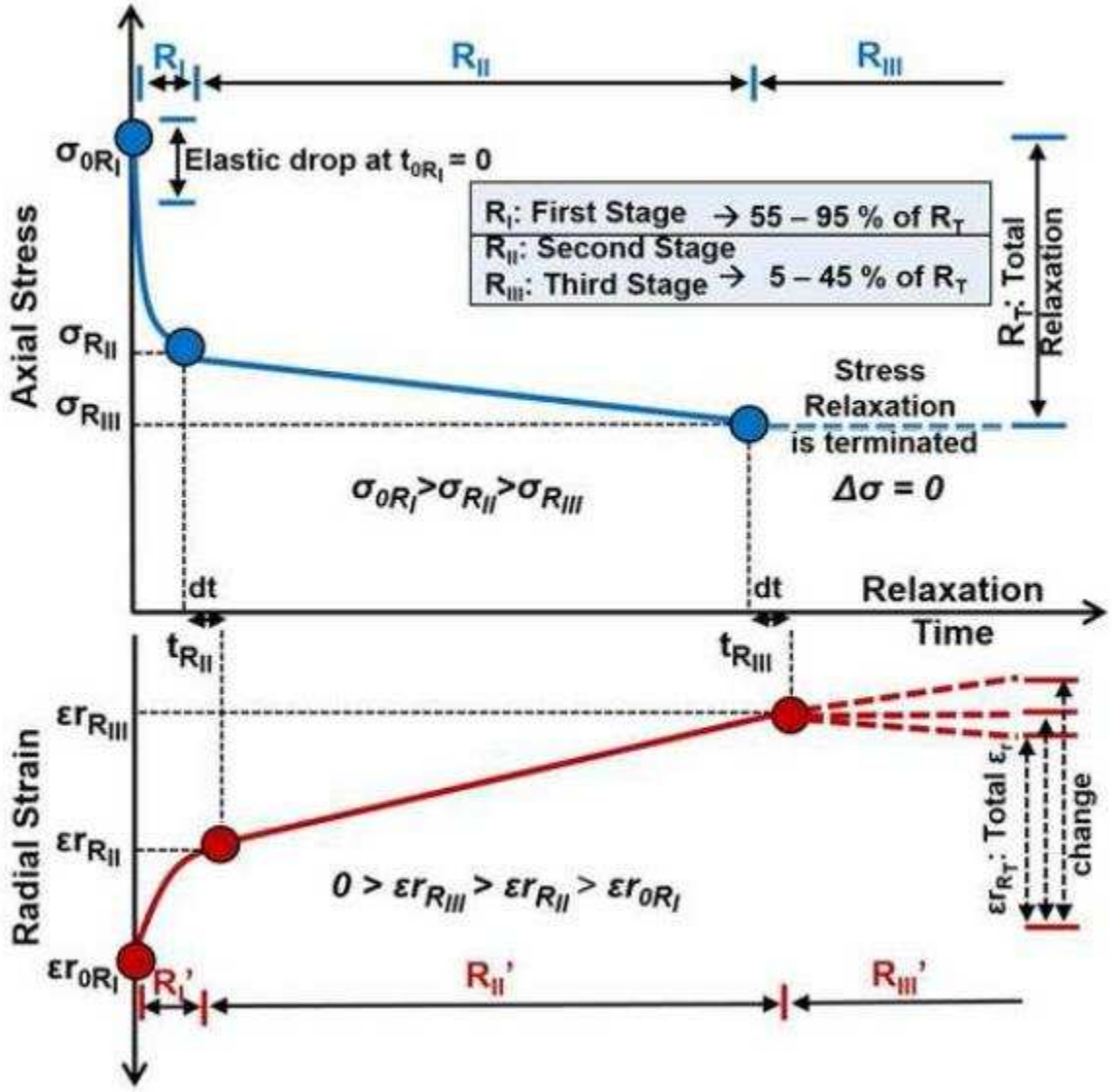

Fig. 15

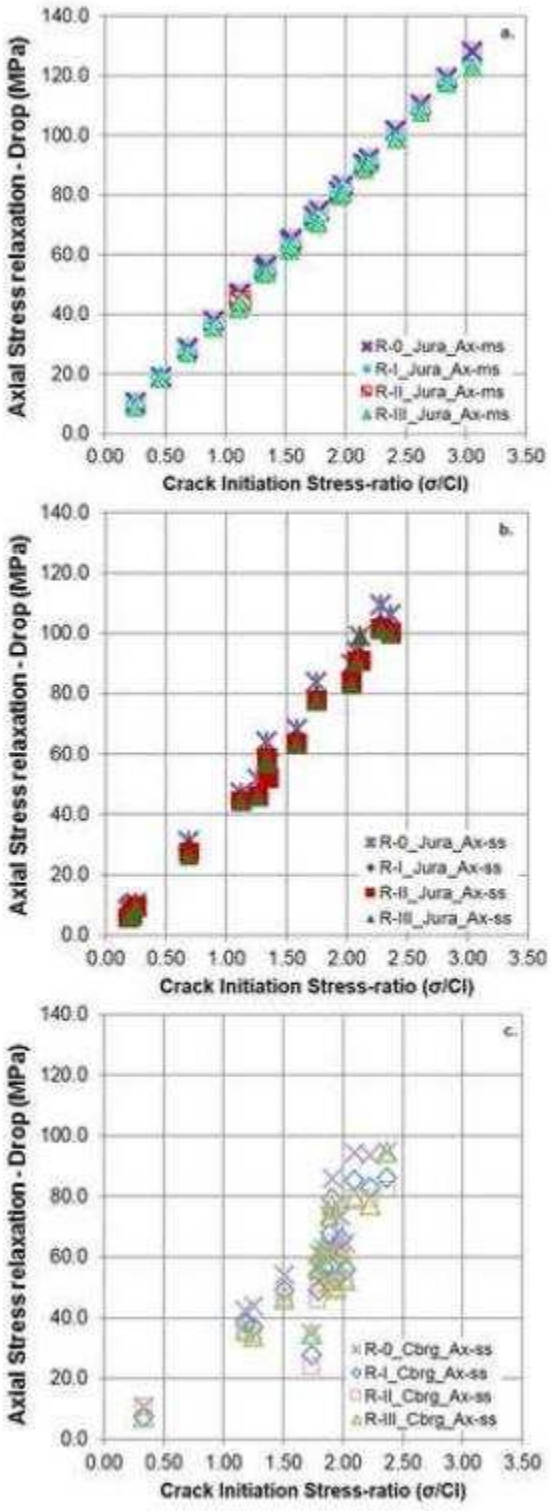

Fig. 16

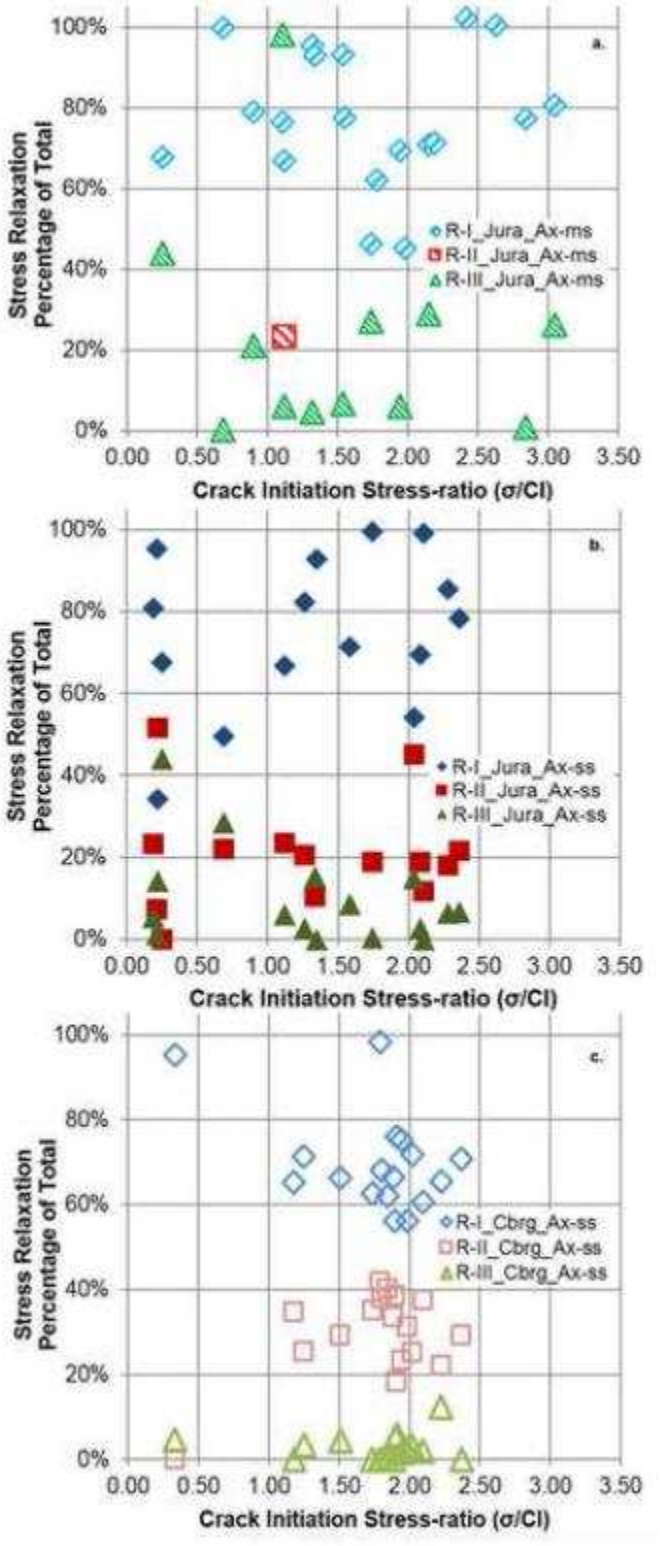

Fig. 17

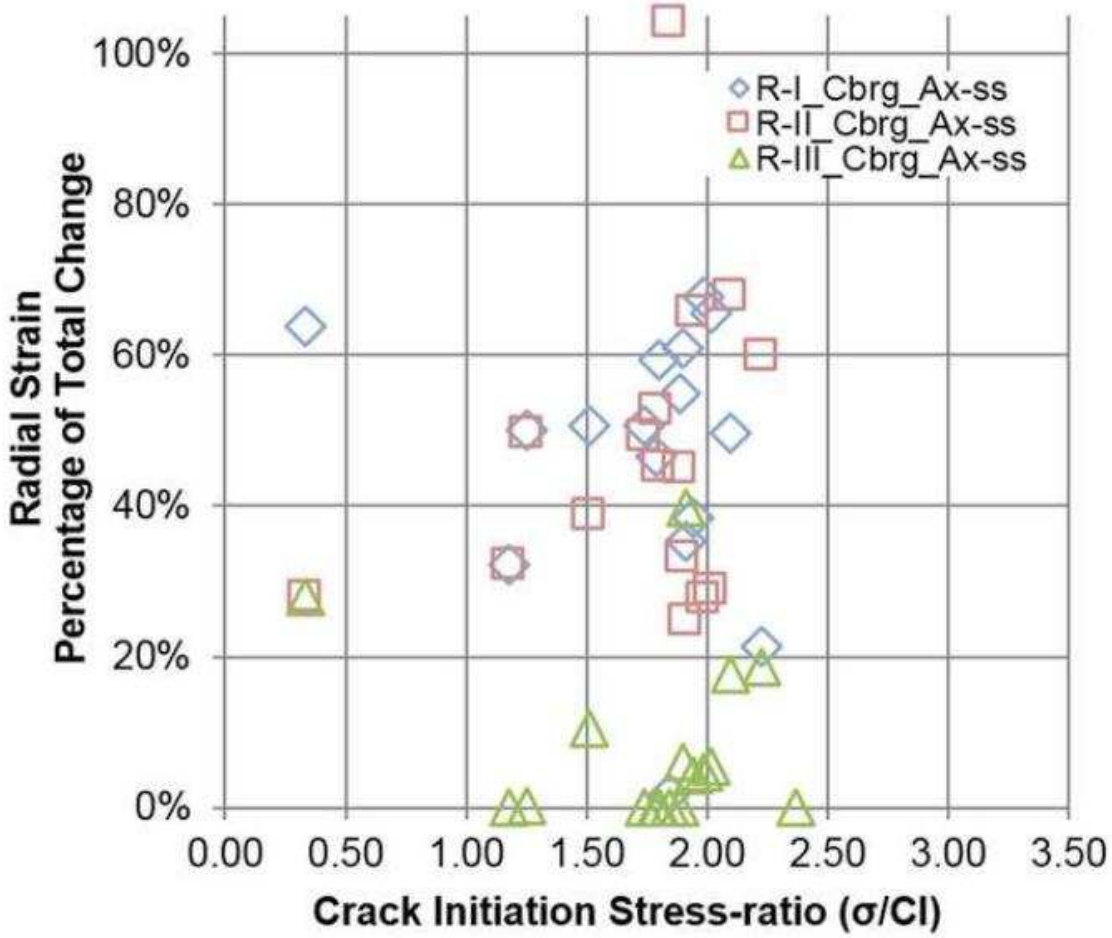

Fig. 18

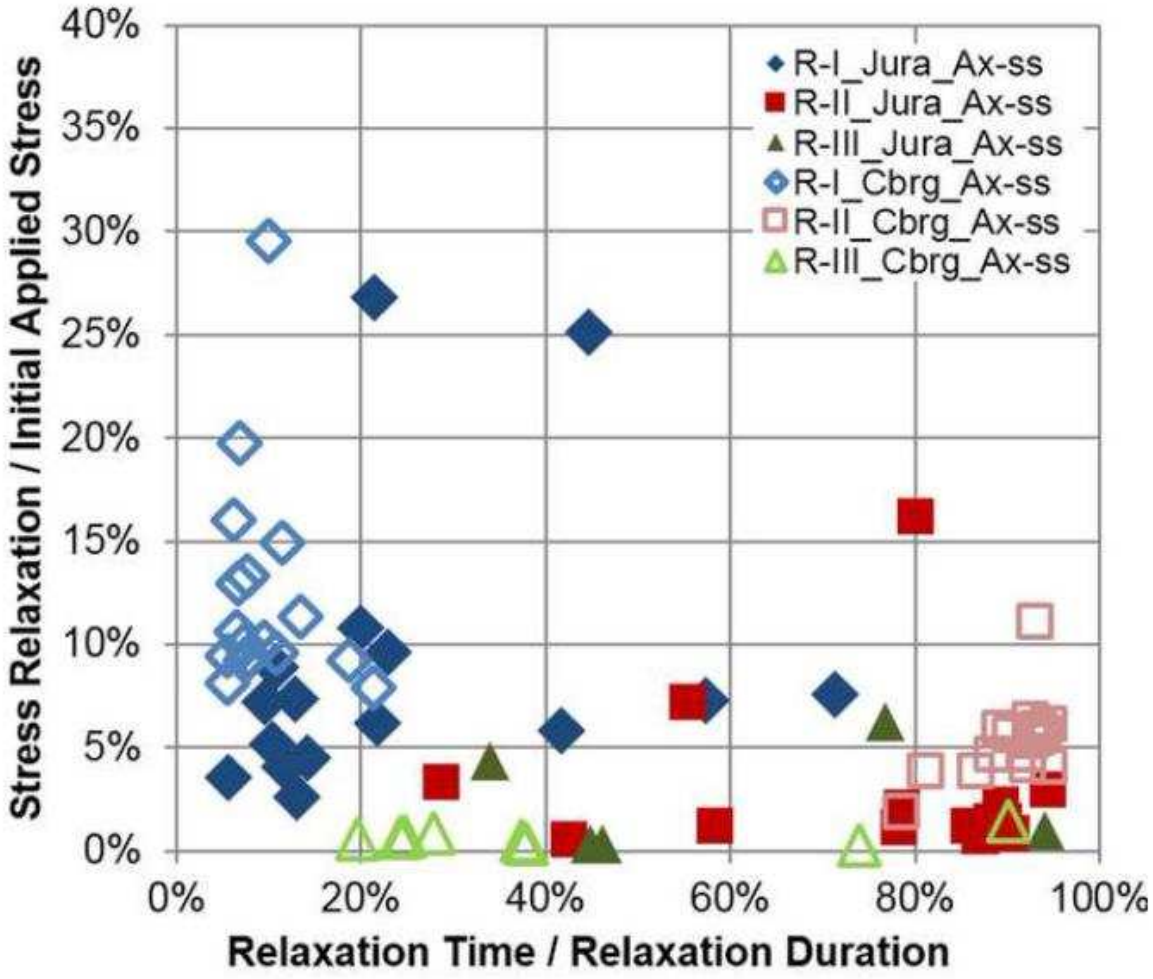

Fig. 19

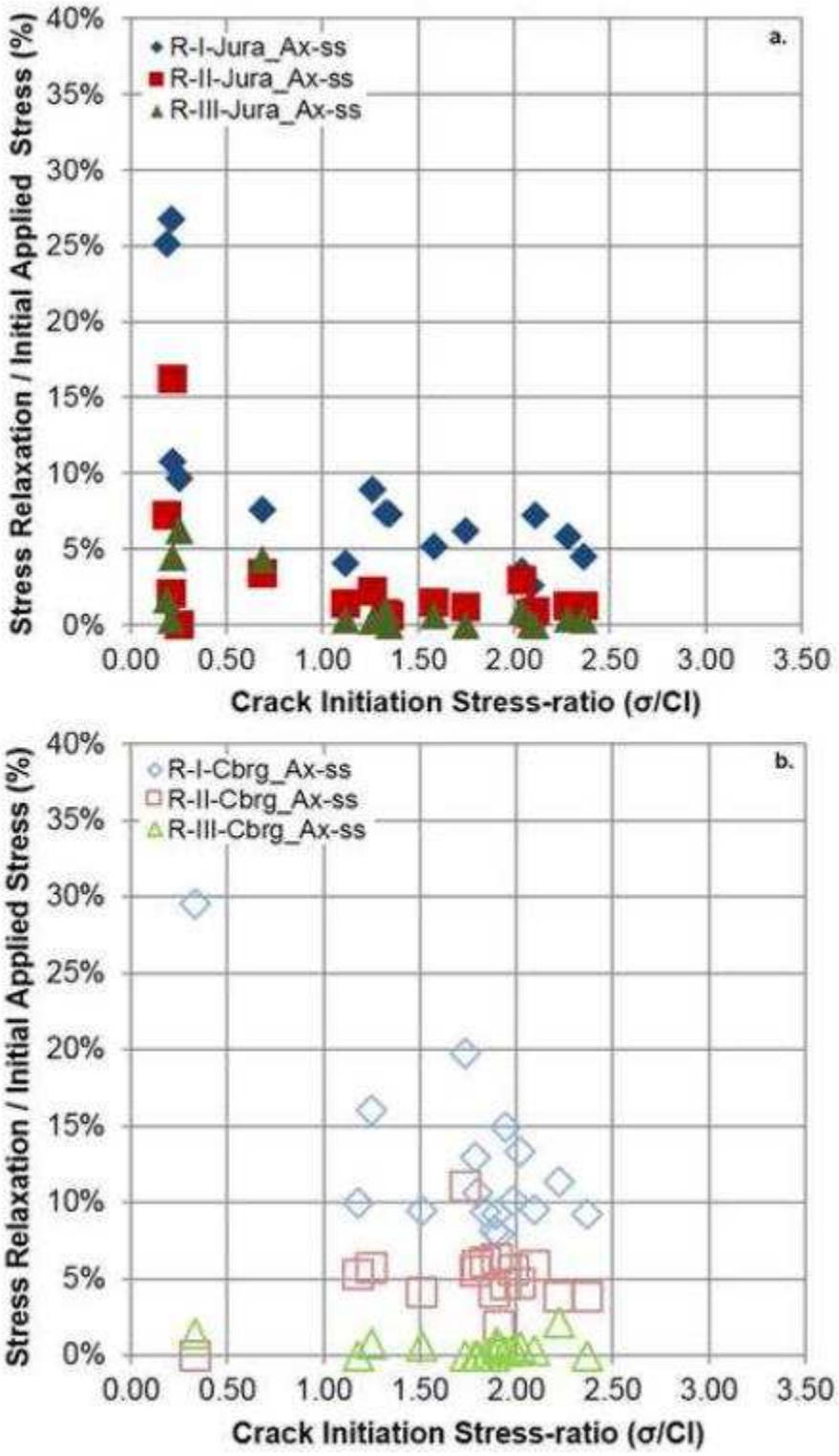

Fig. 20

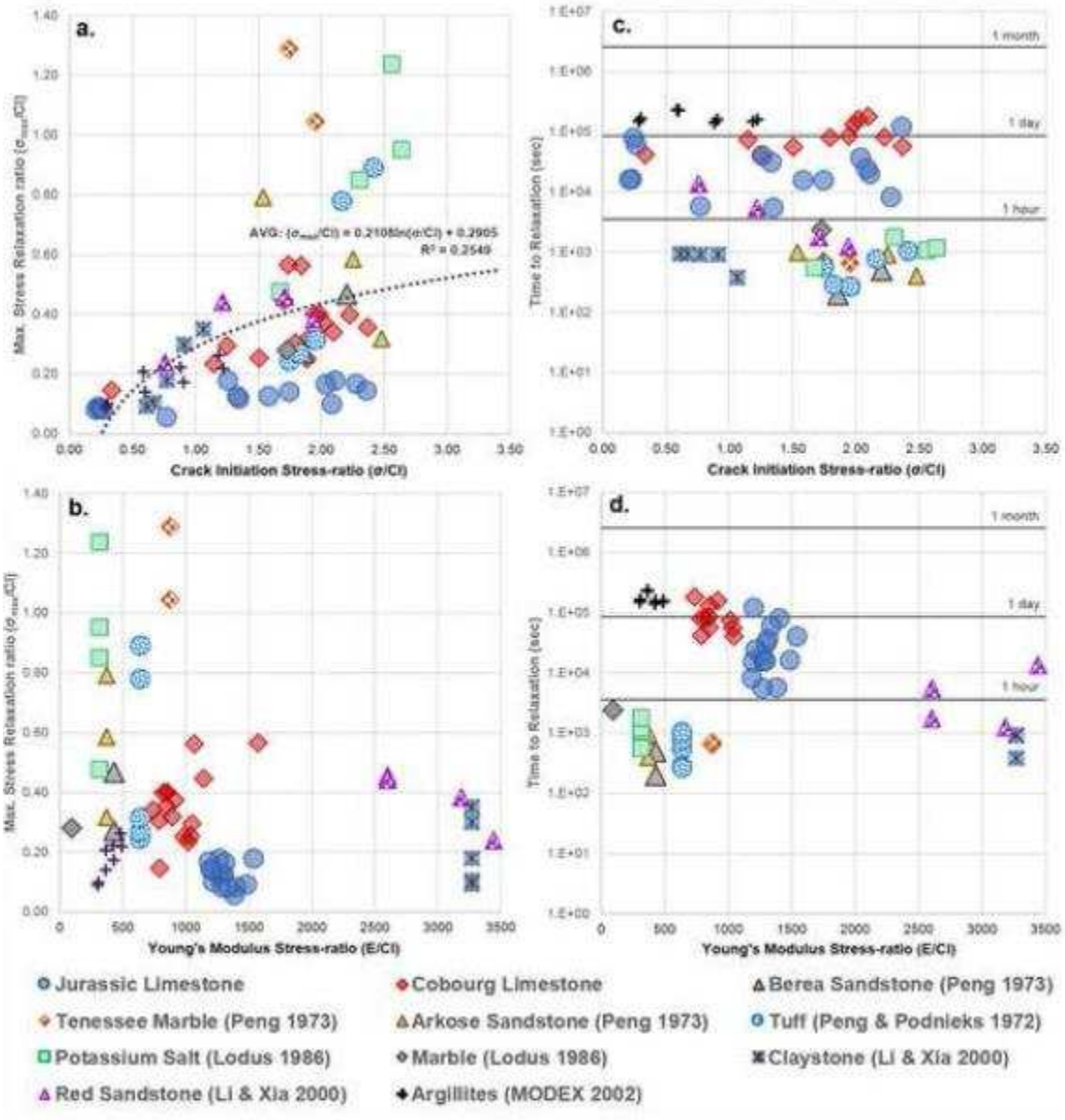

Fig. 21

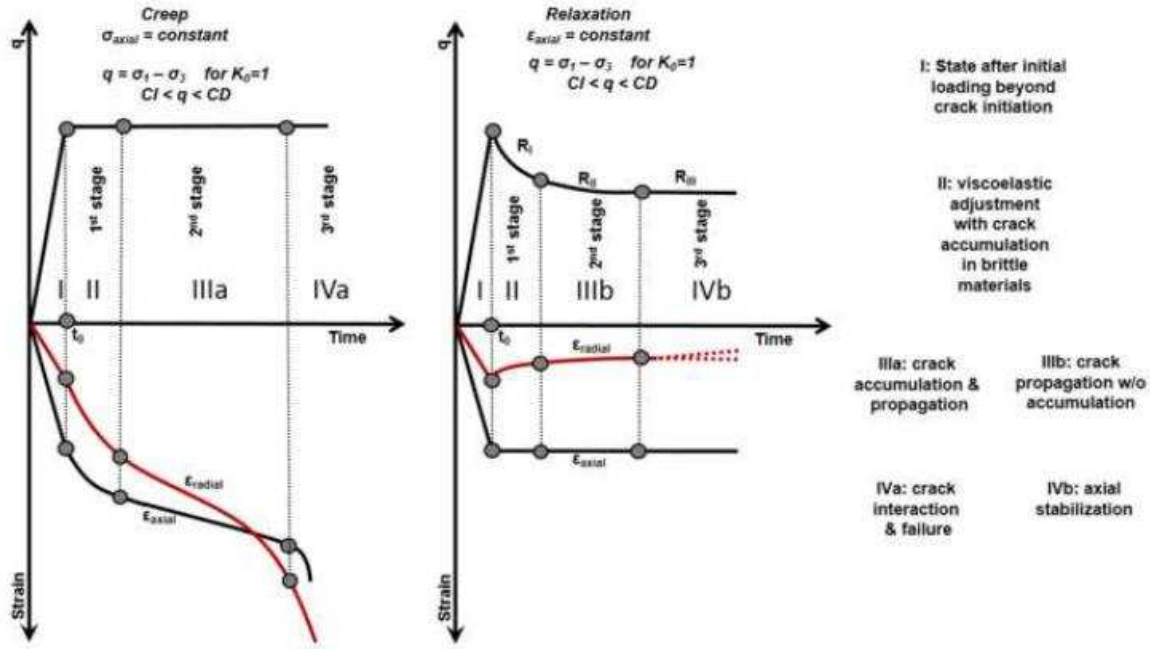

Highlghts

- We give insight into the time-dependent behaviour of rock materials and the importance of performing laboratory testing.
- The testing and analysis presented herein focus on stress relaxation testing on brittle rocks, i.e., the time-dependent response of rock under constant (controlled) strain.
- We show that three distinct stages during stress relaxation take place.
- We present a data set of stress relaxation test results from various rock types to estimate and predict the relaxation behaviour of different rock types.